ISSN 1674-8484 汽车安全与节能学报，第 10 卷 第 3 期，2019 年 1/15
CN 11-5904/U J Automotive Safety and Energy, Vol. 10 No. 3, 2019 249－272

Review and Some Perspectives on Different Methods to Estimate State of Charge of Lithium-Ion Batteries

Gregory L. Plett

(*Department of Electrical and Computer Engineering, University of Colorado Colorado Springs,* Colorado Springs, CO 80918, United States of America)

Abstract: Battery-management systems (BMS) must continuously update estimates of state-of-charge (SOC) in order to compute and calibrate estimates of state-of-health, state-of-energy, and state-of-power (state-of-function), and to prevent cell overcharge and undercharge conditions. There are many methods used to estimate SOC, with some having advantages over others. This paper reviews different SOC-estimation approaches for lithium-ion batteries and hopes to provide the reader with perspectives and insights based on experience working in the field. The physical significance of SOC was described, which can help distinguish between methods to estimate physical SOC versus engineering SOC. Different estimation approaches were discussed in some detail. The problem of defining a battery-pack SOC metric was presented and effcient methods to compute cell SOC for every cell in the pack were reviewed. Finally, some perspectives on the present state of the art and on needed future work in the area were presented.

Key words: lithium-ion-battery; battery-management systems (BMS); state-of-charge (SOC); review; model-based estimation; data-based estimation

锂离子电池荷电状态不同估算方法的综述及讨论（英文）

Gregory L. Plett

（科罗拉多大学 科罗拉多斯普林斯电气及计算机工程系，科罗拉多 斯普林斯 80918，美国）

摘 要：综述了锂离子电池荷电状态（SOC）的不同估算方法，希望能够结合作者在该领域的经验为读者提供一些见解和研究视角。电池管理系统（BMS）需要不断更新电池 SOC 的估计值，用于计算和修正电池健康状态、能量状态以及功率状态（功能状态），并防止电池出现过充或者过放情况。已有许多方法用于估计电池的 SOC，其中有些方法更具优势。该文解说了电池 SOC 的物理含义，有助于区分真实 SOC 以及工程 SOC 的估算方法；对于不同的估计方法进行了较为详细的讨论；并介绍了电池包 SOC 指标的定义问题以及电池包中每个单体电池的 SOC 计算方法；最后，评述了目前该领域的研究前沿，并展望了未来需要开展的工作。

关键词：锂离子电池；电池管理系统（BMS）；荷电状态（SOC）；综述；基于模型的估计；基于数据的估计

中图分类号：TM 911 **文献标志码：**A DOI: 10.3969/j.issn.1674-8484.2019.03.001

收稿日期 / Received：2019-08-22。
基金项目 / Supported by：University of Colorado Colorado Springs Internal Funding。
第一作者 / First author：Gregory L. Plett, Professor, Department of Electrical and Computer Engineering; Director, GATE Center of Excellence in Innovative Drivetrains in Electric Automotive Technology Education University of Colorado Colorado Springs。E-mail: gplett@uccs.edu。

Battery-management systems (BMS) must continuously update estimates of state-of-charge (SOC) and state-of-health (SOH) for all cells in the battery pack, as well as state-of-energy (SOE) and state-of-power (SOP) or state-of-function (SOF) for the pack as a whole. Knowledge of SOC is especially fundamental, since SOC is needed to calibrate many SOH estimates, and in the calculation of SOE and SOP themselves. Knowing SOC is important to avoid overcharge and undercharge conditions, for charge control in general, and for balancing.

Battery-cell SOC quantifies how much charge is stored that might be released to a load circuit to accomplish some task. In some ways, a SOC indicator on a battery-powered system is similar to the fuel gauge on the dashboard of a vehicle. However, while the level of fuel in a tank may be measured directly, there is no practical sensor that can measure SOC; instead, its value must be estimated using more basic measurements of cell voltage, current, and temperature (for example). There are many methods in use to estimate SOC, some giving better estimates than others and some demanding more computation than others. An accurate SOC estimate provides the following benefits [1]:

Longevity: If a fuel tank is over-filled or run empty, the tank is not harmed. However, overcharging or over-discharging a battery cell may cause permanent damage and result in reduced lifetime. An accurate SOC estimate may be used to inform a strategy for battery management to avoid harming cells by not permitting current to be passed that would cause damage.

Performance: Without a good SOC estimator, one must be overly conservative when using the battery pack to avoid over/undercharge due to trusting the poor estimate. With a good estimate, especially one that is provided with reliable confidence bounds, one can aggressively use the entire pack capacity.

Reliability: A poor SOC estimator behaves differently for different load profiles. A good SOC estimator is consistent and dependable, enhancing overall power-system reliability.

Density: Accurate SOC and battery state information allows the battery pack to be used aggressively within the design limits, so the pack does not need to be over-engineered. This allows smaller, lighter battery packs.

Economy: Smaller battery systems cost less. Warranty service on a simpler reliable system costs less.

This paper reviews different methods to estimate SOC for lithium-ion batteries. This review is not intended to supplant previous excellent survey works (e.g., [2–8]) but instead the hope is to provide some additional perspectives and insights based on experience working in the field that may help the reader avoid some common misconceptions and mistakes.

This paper first presents the physical significance of SOC, which leads to steps that can be taken in the laboratory to calibrate tests to provide "truth" SOC against which to validate an estimation method. "Physical SOC" and "engineering SOC" are contrasted, showing why estimating physical SOC is the more reasonable approach. A taxonomy of estimation methods is then presented, and the different approaches are discussed in some detail. The problem of defining a battery-pack SOC metric is introduced, and several efficient methods to accomplish such a goal are described. The paper concludes with a discussion and summary.

1 Definition of SOC

1.1 Physical significance

Battery-cell SOC is a physical quantity that could—in principle—be measured exactly, although no practical sensor exists today that can measure it directly. Still, having a basic knowledge of how lithium-ion battery cells operate is helpful to gain an appreciation for the significance of SOC and for understanding the different estimation methods.

Figure 1 illustrates the principal components of a lithium-ion cell. The cell has a negative electrode (often called the "anode") and a positive electrode (the "cathode"). The electrodes both comprise myriad small particles that can store lithium, and the pore openings surrounding the particles are filled with an electrolyte medium. The particles are adhered to metal-foil current collectors—which themselves are connected to the cell's external terminals—to provide a pathway for electrons to flow between the individual electrodes and the exterior of the cell. The electrodes are mechanically held apart by a separator, which has electrolyte-filled pore openings that are large enough that lithium ions are able to traverse from one electrode region of the cell to the other through the electrolyte but also small enough that particles from one electrode cannot contact particles from the other electrode (which would cause an internal short circuit and most likely result in thermal runaway and fire).

The electrode materials have crystal structures that themselves

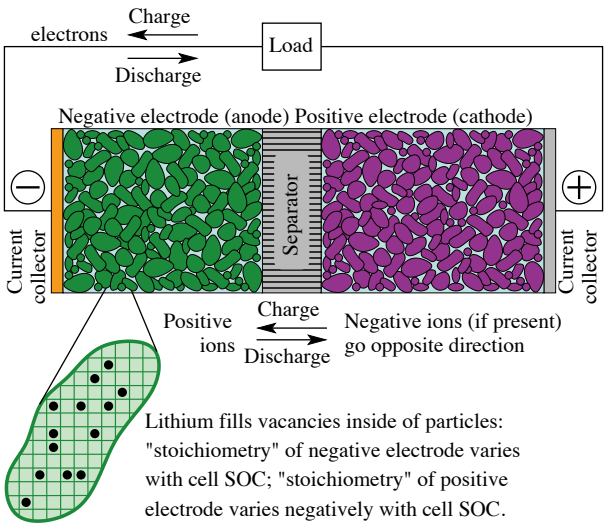

Figure 1 Physical understanding of lithium-ion battery cell operation including physical significance of SOC

have interior pathways into which lithium can enter and move around. The particles store lithium much like a sponge stores water. No permanent chemical change occurs when the cell is charged and discharged; instead, lithium leaves particles from one electrode and enters particles from the opposite electrode. This back-and-forth movement of lithium between electrodes led to the early term "rocking-chair" applied to lithium-ion cells.

Specifically, when a cell is discharging, lithium exits particles from the negative electrode, giving up an electron to the external circuit and a positively charged lithium ion to the electrolyte. The positive ion moves through the electrolyte (primarily via a diffusion mechanism) from the negative-electrode region of the cell to the positive-electrode regions. While lithium ions are moving through the electrolyte, the electron moves through the external circuit and provides energy to the load. It then enters the positive electrode, combines with a positively charged lithium ion from the electrolyte, and enters a positive-electrode particle. When a cell is being charged, the reverse process occurs, as the charger injects electrical energy into the cell.

A key point for our purposes in this paper is to note that the particles in the negative and positive electrodes have a finite discrete number of lithium storage locations. This is illustrated in Fig. 1 by a "zoom" on one negative-electrode particle where these storage locations are represented by a grid, where some locations are filled with lithium (the black circles) and some are not. If we were able to count the number of storage locations filled with lithium versus the number of vacant locations, we could compute an exact SOC. This is not possible with practical BMS equipment, but the idea can provide some helpful ways to think about SOC.

The "stoichiometry" θ^{r} of an electrode (where cell region "r" is "n" for the negative electrode and "p" for the positive electrode) is defined to be the fraction of these storage sites that are filled with lithium, such that $0 \leqslant \theta^{\mathrm{r}} \leqslant 1$. In practice, we never completely fill an electrode with lithium ($\theta^{\mathrm{r}}=1$) or completely empty an electrode ($\theta^{\mathrm{r}} = 0$) because doing so would increase electrochemical and physical stress factors beyond acceptable levels and lead to rapid premature degradation/aging of the cell. Instead, θ^{r} is designed to operate within some region that is narrower than 0...1. We can define $\theta^{\mathrm{r}}_{100}$ to be the stoichiometry of an electrode when the cell is at 100% SOC (i.e., fully charged) and θ^{r}_{0} to be the stoichiometry when the cell is at 0% SOC (i.e., fully discharged). In the negative electrode, $0 < \theta^{\mathrm{n}}_{0} < \theta^{\mathrm{n}}_{100} < 1$ and in the positive electrode $0 < \theta^{\mathrm{p}}_{100} < \theta^{\mathrm{p}}_{0} < 1$.

With this background, it is possible to define a simple equation for the cell SOC. We can write cell SOC z as either

$$z = \frac{\theta^{\mathrm{n}} - \theta^{\mathrm{n}}_0}{\theta^{\mathrm{n}}_{100} - \theta^{\mathrm{n}}_0} = \frac{\theta^{\mathrm{p}} - \theta^{\mathrm{p}}_0}{\theta^{\mathrm{p}}_{100} - \theta^{\mathrm{p}}_0}.$$

If it were possible to measure θ^{r} using practical equipment, then it would be straightforward to calculate SOC using this expression. Since it is not possible to do so, we seek other approaches.

We notice that it is also possible to define a simple equation for electrode *total capacity* (in ampere-hours):

$$Q^{\mathrm{r}} = \varepsilon^{\mathrm{r}}_{\mathrm{s}} A L^{\mathrm{r}} c^{\mathrm{r}}_{\mathrm{s,max}} \left|\theta^{\mathrm{r}}_{100} - \theta^{\mathrm{r}}_{0}\right| F / (3\,600). \quad (1)$$

In Eq. (1), A is the current-collector surface area and L^{r} is the thickness of the electrode. So, AL^{r} is the total volume occupied by the electrode. However, only some of this volume is occupied by the solid electrode particles since some is occupied by the electrolyte and conductive additives and binder and so forth. The volume fraction of the solid $0 < \varepsilon^{\mathrm{r}}_{\mathrm{s}} < 1$ is the fraction of the electrode volume that is occupied by the electrode active materials (the particles). Therefore, $\varepsilon^{\mathrm{r}}_{\mathrm{s}} AL^{\mathrm{r}}$ is the volume of the active materials in an electrode. This quantity is then multiplied by $c^{\mathrm{r}}_{\mathrm{s,max}}$ which is the maximum concentration of vacant sites in the electrode materials that are able to hold lithium. This quantity is multiplied by $|\theta^{\mathrm{r}}_{100} - \theta^{\mathrm{r}}_{0}|$ to reflect the fact that not all of these sites are ever used, but rather a range of stoichiometries is used. The quantity computed so far is a valid measure of cell total capacity, measured in moles. To convert from moles to ampere-hours, we must multiply by F (Faraday's constant—to convert from moles to ampere-seconds) and divide by 3600 (to convert ampere-seconds to ampere-hours). In operation, Q^{n} is equal to Q^{p} since both quantities represent the maximum amount of lithium that can be transferred from one electrode to the other (and back) while cycling.

We can also define an equation for the *residual capacity* of an electrode (in ampere-hours):

$$Q^{\mathrm{r}}_{\mathrm{resid}} = \varepsilon^{\mathrm{r}}_{\mathrm{s}} A L^{\mathrm{r}} c^{\mathrm{r}}_{\mathrm{s,max}} \left|\theta^{\mathrm{r}} - \theta^{\mathrm{r}}_{0}\right| F / (3\,600).$$

This is the quantity of charge that can be removed from the electrode before the cell has SOC of 0%. Therefore, we can relate cell SOC to capacities as $z = Q^{\mathrm{r}}_{\mathrm{resid}} / Q^{\mathrm{r}}$.

We are getting closer to an equation that we can use to describe SOC in a more practical way. But, before we proceed, notice that the total capacity of the cell is a physical quantity related to the finite discrete number of storage sites for lithium in the electrode. This quantity does not vary with temperature or C-rate of cell usage. (The *total capacity* of the cell is different from the *discharge capacity* of the cell—which does vary with temperature and C-rate—as discussed later.) The total capacity of the cell can change only if any of the terms in Eq. (1) change: $c_{\mathrm{s,max}}$, F, and 3 600 are physical constants that don't change; A and L^{r} are geometric quantities that are assumed not to change; so, total capacity can change only if $\varepsilon^{\mathrm{r}}_{\mathrm{s}}$ or $|\theta^{\mathrm{r}}_{100} - \theta^{\mathrm{r}}_{0}|$ change. As the cell ages, the volume fraction of active material can decrease if the material itself breaks down in some way (i.e., storage sites for lithium are lost). The stoichiometric operating window $|\theta^{\mathrm{r}}_{100} - \theta^{\mathrm{r}}_{0}|$ can also shrink due to side reactions consuming lithium such that not all lithium exiting one electrode enters the other electrode but is instead lost permanently to side-reaction products (such as lithium plating or solid–electrolyte interphase layer growth [9-10]). The first category of degradation mechanism is referred to as "loss

of active material" (LAM) in the literature and the second category is called "loss of lithium inventory" (LLI). This paper does not concern itself with a detailed understanding of capacity degradation, which is itself estimated by state-of-health algorithms, but it is still helpful to have this general understanding of capacity loss when considering how well an SOC-estimation algorithm might work over the lifetime of a cell as its total capacity changes.

As a cell is cycled, the movement of lithium between electrodes internal to the cell is matched by the movement of electrons external to the cell. Therefore, there is a direct connection between measured electrical current and a change in SOC. Further, cell voltage is related, in part, to the stoichiometries of the electrodes. However, there are several other factors involved and so voltage by itself is not a good indicator of SOC. For example, one of these factors is that cells have physical internal resistance and so the cell terminal voltage is equal to some internal voltage minus an ohmic voltage drop across this resistance. It is the internal voltage that is more indicative of cell SOC than the terminal voltage. The internal and external voltages of the cell can approach each other when the cell is in equilibrium (one that has been "open circuit" for an extended period of time). This *open-circuit voltage* (OCV) has a relationship with SOC that can help estimate SOC, as described later. Generally, the OCV of a cell increases as the SOC of the cell increases such that the minimum OCV is encountered at the minimum SOC and the maximum OCV is encountered at the maximum SOC. The OCV of a cell is a weak function of temperature and also changes somewhat as the cell ages if capacity is lost due to side reactions that cause a shift in the electrode stoichiometric operating windows.

1.2 Working definitions related to SOC

With an understanding of the physical significance of SOC, it is possible to create some working definitions of related quantities that are themselves related to measurable values. These definitions are illustrated in Fig. 2.

Definition: A cell is *fully charged* when its OCV is equal to $v_{max}(T)$. Notice that v_{max} is a function of temperature, T, although cell manufacturers often specify v_{max} only at 25 ℃.

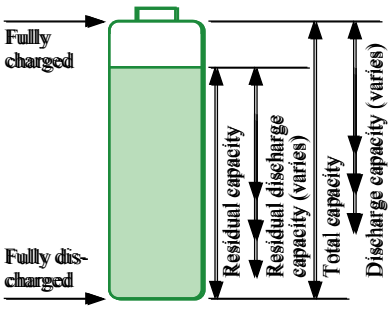

Figure 2 Illustrating important definitions relevant to understanding SOC

To achieve a desired OCV in a laboratory setting, the cell is charged with a current that tapers to infinitesimal levels such that terminal voltage $v(t) = v_{max}(T)$ and the applied current approaches zero at the end of charging. A fully charged cell has SOC of 100%. Therefore, we can calibrate laboratory tests to a 100% SOC point by fully charging the cell.

Definition: A cell is *fully discharged* when its OCV is equal to $v_{min}(T)$ (e.g., after being discharged at infinitesimal current levels). Notice also that v_{min} is a function of temperature, T, although cell manufacturers often specify v_{min} only at 25 ℃. A fully discharged cell has SOC of 0%. Therefore, we can calibrate laboratory tests to a 0% SOC point by fully discharging the cell.

Definition: The *total capacity* Q of a cell is the quantity of charge (often measured in ampere-hours) removed from a cell as it is brought from a fully charged state to a fully discharged state.

Definition: The *discharge capacity* $Q_{[rate]}$ of a cell is the quantity of charge removed from a cell as it is discharged at a constant rate from a fully charged state until its loaded terminal voltage reaches $v_{min}(T)$. Because the discharge capacity is determined based on loaded terminal voltage rather than OCV, it is strongly dependent on the cell's internal resistance, which itself is a function of rate and temperature. Hence, the discharge capacity of a cell is rate-dependent and temperature-dependent. Because of the resistive $I \times R$ drop, the discharge capacity is less than the total capacity unless the discharge rate is infinitesimal. Likewise, the SOC of the cell is nonzero when the terminal voltage reaches $v_{min}(T)$ at a non-infinitesimal rate.

Definition: The *nominal capacity* Q_{nom} of a cell is a manufacturer-specified quantity that is intended to be representative of the 1C-rate discharge capacity Q_{1C} of a particular manufactured lot of cells at room temperature, 25 ℃. The nominal capacity is a constant value. Since the nominal capacity is representative of a lot of cells and the discharge capacity is representative of a single individual cell, $Q_{nom} \neq Q_{1C}$ in general, even at beginning of life. Also, since Q_{nom} is representative of a discharge capacity and not a total capacity, $Q_{nom} \neq Q$.

Definition: The *residual capacity* of a cell is the quantity of charge that would be removed from a cell if it were brought from its present state to a fully discharged state.

Definition: The *residual discharge capacity* of a cell is the quantity of charge that would be removed from the cell if it were brought from its present state under a constant discharge current to the point where the loaded terminal voltage reaches $v_{min}(T)$. This is less than the residual capacity.

Definition: The *state-of-charge* of a cell is the ratio of its residual capacity to its total capacity.

With these definitions in place, relating lithium movement internal to the cell to electron movement outside the cell, we can create a mathematical model for SOC:

$$z(t) = z(0) - \frac{1}{Q}\int_0^t \eta(t)i(t)\,\mathrm{d}t\,, \tag{2}$$

where $z(t)$ is the cell SOC at time t, $i(t)$ is instantaneous cell current (assumed positive for discharge, negative for charge), and Q is the cell total capacity (in ampere-seconds). Cell coulombic efficiency $\eta(t)$ models the fraction of charging current that contributes to changing SOC: it is generally assumed that $\eta(t) = 1$ for every moment in time that the external current is in the discharge direction and $\eta(t) \leqslant 1$ for every moment in time the externally applied current is charging the cell. Note that the coulombic efficiency for lithium-ion cells is generally very high, often greater than 0.99, and models the quantity of charge that can be removed from the cell divided by the quantity of charge that has been added to the cell. It is different from energy efficiency, which is the energy that can be removed divided by the energy that has been added to the cell. Energy efficiency is computed considering the losses due to resistive heating of the cell; coulombic efficiency instead refers to losses of lithium due to reversible or irreversible side reactions that do not contribute to charging the cell. Equation (2) writes total capacity Q as a constant, but as we have already discussed, it is a very slowly changing quantity, generally decreasing as the cell ages.

1.3 Physical state of charge versus engineering state of charge

Until this point, we have considered a physical definition of SOC (PSOC). This has the advantage of a simple definition and a simple mathematical model involving constant quantities (neglecting that total capacity changes slowly as the cell ages). However, from an engineering perspective, this definition may not always be satisfying. For example, consider a simple application that requires a constant discharge current. The cell will reach a minimum terminal voltage before it reaches a minimum open-circuit voltage (and therefore a minimum PSOC) because of the voltage drop across the internal impedance of the cell. Perhaps the minimum terminal voltage is reached when the PSOC is equal to 10%. Then, only 90% of the cell capacity is usable by the application. In that sense, if the SOC estimate is intended as an "fuel gauge" indicator for the cell, then the PSOC may be a misleading indicator of how much operational time remains for the application: in this example, there is actually zero runtime remaining when the PSOC is 10%.

Some researchers propose "engineering state-of-charge" (ESOC) definitions to attempt to mitigate this problem. For example, the USABC Battery Test Procedure Manual defines a cell's SOC as "the ratio of the Ampere hours remaining in a battery at a given rate [Q_{res}] to the rated capacity [Q_{rated}] under the same specified conditions" [11]. In terms of the definitions used in this paper, the USABC ESOC is defined as residual discharge capacity divided by nominal capacity. However, Truchot et al. [12] identify four serious issues with using this ESOC definition in a BMS:

1) The ESOC estimate is not referenced to an absolute scale; as the battery ages, its calibration is not trivial.

2) To calibrate the ESOC scale, the residual discharge capacity of the cell cannot be obtained easily in actual use.

3) The ESOC is defined as a fraction of the nominal capacity. The nominal capacity is a statistical quantity that describes an overall cell design or a manufactured lot of many cells and is not equal to the capacity of the individual cell under consideration. The actual cell capacity might be significantly different from the nominal capacity.

4) In use, the duty cycles and operating conditions experienced by a cell are far more complex and less controlled than those used in the laboratory setting to calibrate the ESOC estimator.

A slightly refined ESOC definition would be to compute the ratio of the residual discharge capacity to the discharge capacity of the cell, but although this resolves the third issue, it further complicates the calibration process required to determine ESOC. Generally, papers that attempt to estimate some kind of ESOC require difficult-to-calibrate Peukert corrections to Eq. (2) and use either nominal capacity or discharge capacity (instead of total capacity) in the denominator of the factor that normalizes the integral term.

How to resolve this issue? As we will see, the better methods for SOC estimation require sets of mathematical equations (otherwise known as "models") of cell input–output (current–voltage) behaviors. If PSOC is known, then these models can be used to compute any desired definition of ESOC in a straightforward manner. The reverse is not generally true: if ESOC is known it may not even be possible to compute PSOC. Therefore, I prefer methods that estimate PSOC and then additionally use that estimate to compute an estimate of ESOC if desired.

In the remainder of the paper, I will not mark a distinction between PSOC and ESOC. Some of the papers that I reference use the PSOC definition; others use some form of ESOC definition. Instead, the focus is on the methods that are used to estimate SOC, which do not generally depend critically on the way that SOC is defined. Therefore, I return to using the generic term SOC instead of either PSOC or ESOC.

2 Methods to estimate SOC

With this background, we can now explore the different methods proposed in the literature for estimating SOC. Fig. 3 shows a taxonomy of these methods. Some ad hoc approaches have been proposed; learning methods are used; and control-systems-inspired observers and adaptive filtering methods are common. These different categories of approaches are described in the following subsections.

2.1 Ad hoc methods

We will first look at a set of single-measurement SOC-estimation methods. We ask the questions: Can a voltage

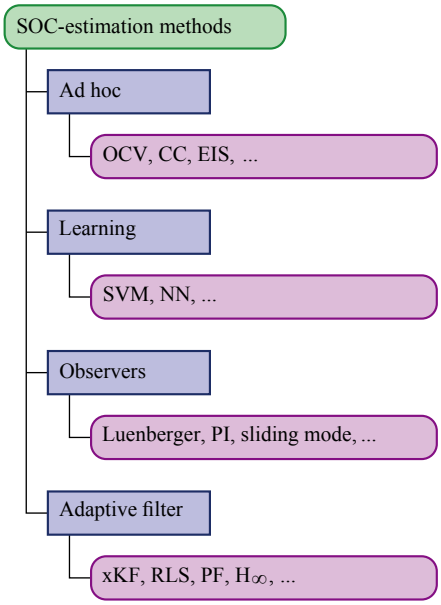

Figure 3 Taxonomy of SOC-estimation methods

measurement be used to infer SOC? Or, can current-sensor measurements be used? Or, can an impedance function be used? Under some conditions, the answer is "yes", although the methods we look at in this section tend to lack the robustness of some of the more advanced methods that are introduced later.

2.1.1 SOC estimation based on OCV

As we have already seen, a cell whose internal electrochemical dynamics are in equilibrium has a measurable terminal voltage that is equal to its OCV. Further, the OCV of a cell is a deterministic function of the cell's SOC, which varies slightly with temperature and somewhat with cell age. If we can determine the OCV of a cell, and if we know the OCV versus SOC relationship of the cell for the present operating conditions, then we can perform a reverse table lookup to find SOC from OCV.

As an example, the OCV versus SOC relationships for five different lithium-ion cells are plotted in Fig. 4. These relationships are different primarily because different materials are used in the positive electrodes of these particular cells and because different electrode stoichiometric windows $|\theta^{r}_{100} - \theta^{r}_{0}|$ are used in each cell design: the lowest-voltage cell (blue line) has an lithium-iron-phosphate (LFP) chemistry; the others include cells having lithium-manganese-oxide (LMO), lithium-cobalt-oxide (LCO), nickel-manganese-cobalt oxide (NMC) in different ratios, nickel-cobalt-aluminum oxide (NCA), and/or possibly some blends of the above.

As an example of how we might determine SOC based on OCV, consider the cell whose OCV versus SOC relationship is plotted as the purple line. If we were to measure an OCV of 4.0 V for this cell, then we could say that the cell's SOC is approximately 77% (if we had an exact functional form or a table of values, we could be more precise).

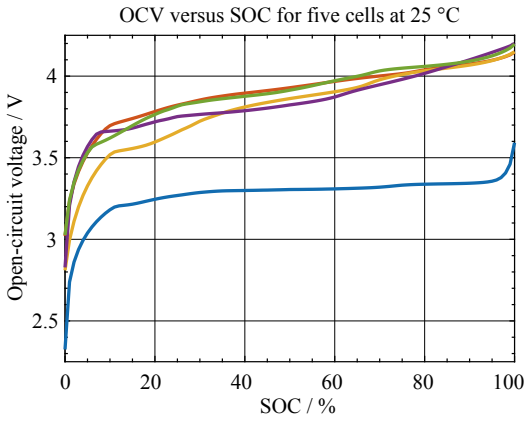

Figure 4 Examples of OCV versus SOC relationships for five different lithium-ion cell designs

Unfortunately, it is very difficult to estimate SOC well using this method since it is extremely difficult to obtain precise measurements of OCV. Generally, the cell is not in equilibrium when SOC estimates are needed, and so some process must be devised to regress the measured voltage—usually through some kind of model of cell dynamics—back to OCV (e.g., [12-17]) in order to determine an estimate of SOC. These processes always have some degree of error. Even if a cell has rested for a long period of time (hours or even days), there can be significant hysteresis in the resting voltage compared to the OCV which is defined by perfect thermodynamic equilibrium [18–24]. This hysteresis introduces error into the OCV estimate, which further introduces error into the SOC estimate.

Notice also from Fig. 4 that the OCV versus SOC relationships have a very shallow slope. This means that small errors in the OCV estimate are magnified to become large errors in an SOC estimate. This is especially true for LFP chemistries: an estimated OCV near 3.3 V might correspond to any SOC between about 30% and 90% for the particular cell in the figure. For this reason, the OCV method by itself is not considered to be adequate for estimating SOC in general. However, it can provide initial SOC estimates for some of the feedback methods described later, based on a resting cell voltage measured on BMS startup when the battery is first connected to the load after a long rest interval.

2.1.2 SOC estimation based on current-sensor integration

As we have already discussed, SOC can be modeled exactly using Eq. (2). Therefore, it might be reasonable to think we could estimate SOC as:

$$\hat{z}(t) = \hat{z}(0) - \frac{1}{\hat{Q}} \int_0^t \hat{\eta}(t) i_{\text{meas}}(t)\, \mathrm{d}t \,, \tag{3}$$

where $\hat{z}$ (t) is an estimate of SOC at time t, $\hat{Q}$ is an estimate of cell total capacity, $\hat{\eta}$ is an estimate of coulombic efficiency, and i_{meas} (t) is measured current. This method is called "coulomb counting" because it is integrating (counting) the charge

(coulombs) into and out of the cell.

Unfortunately, there are some very serious problems with using coulomb counting by itself (although some modifications can help [25-26]). First, we have no way to find $z(0)$ exactly. Even if the battery pack has rested for a long period of time before initializing the coulomb counter, an initial voltage reading will not be exactly the same as OCV, and so there will be some degree of error in the initial SOC estimate. Equation (3) provides no mechanism for correcting this initial error and so the error will propagate unchanged for the entire period of operation of the battery as a constant bias error to the SOC estimate. Second, we never know the cell total capacity Q exactly. There is always some estimation error even using the best total-capacity estimation methods [27-28]. Equation (3) provides no mechanism for correcting for an error in the total-capacity parameter, so the quantity of counted coulombs will be scaled by an incorrect value, resulting an SOC estimate that tends to diverge from the true value over time. Third, coulombic efficiency $\eta(t)$ is never known exactly, and tends to be a complicated function of rate, temperature, and cell age leading to somewhat random errors introduced into the estimate of SOC versus the true value. Finally, and perhaps most importantly, the measured current $i_{\text{meas}}(t)$ of Eq. (3) is not the same as the actual current $i(t)$ of Eq. (2). We can write:

$$i_{\text{meas}}(t) = i(t) + i_{\text{noise}}(t) + i_{\text{bias}}(t) + i_{\text{nonl}}(t) + i_{\text{self disch}}(t) + i_{\text{leak}}(t),$$

where the measured current $i_{\text{meas}}(t)$ is equal to the actual current $i(t)$ plus measurement noise $i_{\text{noise}}(t)$, plus any dc bias in the measurement $i_{\text{bias}}(t)$ from the analog-to-digital (A2D) conversion system, plus nonlinear errors $i_{\text{nonl}}(t)$ introduced into the measurement by the A2D, plus unmeasurable self-discharge current $i_{\text{selfdisch}}(t)$ that affects SOC but does not affect the current-sensor measurement, plus unmeasured leakage current $i_{\text{leak}}(t)$ that is drawn from the cell to power the A2D subsystem. Since $i_{\text{meas}}(t)$ differs from $i(t)$ in unpredictable ways, the uncertainty of an SOC estimate produced by coulomb counting increases over time (alternately, our confidence in the accuracy of the SOC estimate decreases over time).

2.1.3 SOC estimation based on impedance.

A third simple way to estimate SOC is based on a measurement of the cell's impedance, which is made using electrochemical impedance spectroscopy (EIS). A small-amplitude sinusoidal current is injected into the cell, and the perturbation in the terminal voltage caused by this input signal is monitored. The magnitude gain $M(\omega)$ of the amplitude of the output-voltage perturbation versus the input-current amplitude and the phase shift $\phi(\omega)$ between input and output at every frequency ω are combined into a complex impedance function $Z(\omega)=M(\omega)e^{j\phi(\omega)}$. Such impedance functions are often visualized in the literature using Nyquist plots of -Imag $[Z(\omega)]$ versus Real $[Z(\omega)]$ such as in the example drawn in Fig. 5.

Even if this form of diagram is unfamiliar, it should be

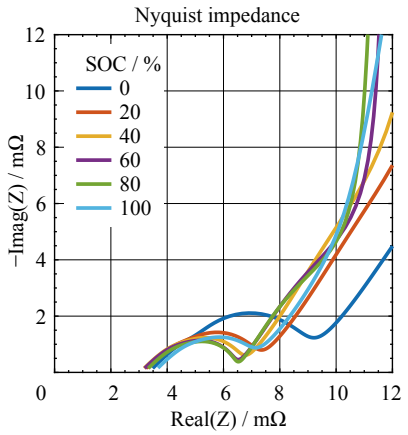

Figure 5 An example Nyquist diagram of cell impedance

evident from the differences between the plotted lines that cell impedance can be a strong function of SOC, so it is reasonable to investigate whether SOC can be estimated directly from EIS data only. Reference [4] notes that the first impedance measurements of batteries appear to have been made by Willihnganz in 1941. It cites Ref. [29], which maps a single-frequency impedance phase to an SOC estimate. The frequency is not stated, nor is the impact of temperature or aging, which are likely to be significant. It also cites reference [30], which assumes a very simple cell model, attaches a reference load, and "measures" the infinite-frequency impedance. It then infers SOC as a table lookup. Reference [2] also surveys EIS for SOC estimation, mostly prior to lithium-ion chemistries. The authors claim that features on the "bump" in the Nyquist plot are essentially linear with SOC, but it is unclear how differences in temperature and cell aging will change this result. Reference [31] fits 1 Hz to 15 kHz frequency range EIS (5 s measurement time per frequency) to a simple equivalent-circuit cell model, then fits values for the circuit parameters to the EIS data, making exponential fits of parameters versus SOC. SOC is inferred by table lookup from these data. Again, is unclear how different temperatures and aging affect this result. Some other references that consider SOC estimation via impedance methods include [32-37].

There are some significant challenges to using EIS data in an SOC estimator. First, a fundamental assumption when finding a frequency response is that the cell is in an equilibrium state. If the cell must be at rest for several hours to approximate an equilibrium condition before the measurement is made, this severely restricts the benefit of any purely EIS-based SOC-estimation method. Further, Ref. [6] notes that an ac signal generator is required, which increases BMS cost; impedance has a complicated relationship with SOC and there are many influencing factors (including nonuniformity of internal resistance); impedance is very small, so is difficult to determine with accuracy in-situ; and resistance varies very little over a broad range, diluting the accuracy of SOC estimate. In particular, the dependence of impedance on SOC

is usually smaller than the dependence on temperature [4].

It seems that EIS may not be a good *direct* estimator of SOC. While impedance is clearly a function of SOC, we generally cannot allow the cell to rest for long periods every time we require an SOC estimate. Without further modeling and robust online parameter-update means, we do not know how a cell's SOC versus impedance map evolves as the cell ages. Further, temperature is a significant contributor that may dominate the SOC effects in most cases. While some papers claim that high-frequency resistance is strongly SOC-dependent and can be used to determine SOC, others claim that it is independent of SOC—this observation of such different results from different research teams probably indicates a large dependence on a cell's specific chemistry and design. However, frequency response—especially if it can be determined economically using specialized electronics and processing in the future—may be able to augment other SOC-estimation methods as an independent "sensor" of SOC to help fine-tune results.

2.2 Learning methods

As we discussed earlier, coulomb counting is not a robust method for SOC estimation in a BMS. However, it can be a good method for calculating SOC versus time for laboratory experiments if the cell being tested has well-calibrated total capacity, initial SOC, and columbic efficiencies, and if the measurement equipment has high accuracy (e.g., see Chapter 2 in [38] or Topic 2 in [39] for calibration methods). Therefore, it is possible to collect datasets that comprise profiles of voltage, current, surface temperature, and SOC versus time from a cell for which we would like to make an accurate SOC estimator.

One category of SOC estimators that uses such datasets directly is labeled as "Learning" methods in Fig. 3. These are "black-box" approaches as illustrated in Fig. 6; namely, they are functional mappings between inputs (current, voltage, and temperature) and outputs (SOC) that can be created using training data but without any application-specific knowledge of the internal workings of the system being modeled.

To employ these methods, the designer must first select a mathematical-function form that is generic enough that

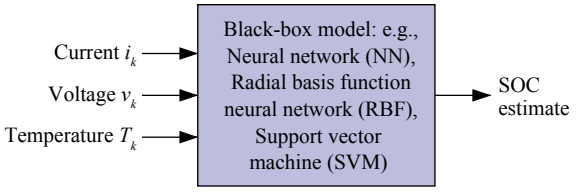

Figure 6 Generic view of learning methods for SOC estimation

its parameter values can be adjusted to model the desired relationship without changing the equations themselves; then, the parameters must be tuned so that the black-box model "learns" to reproduce the SOC from the lab-test datasets given the lab-test inputs. Different types of learning architectures can be selected, including support-vector machines (SVMs), perceptron-based neural networks (NNs), and radial-basis-function neural networks (RBF). In [40], Hansen and Wang propose a support-vector machine of the form

$$\hat{z} = \sum_{i=1}^{N}(\alpha_i - \alpha_i^*)K(\boldsymbol{x}_i, \boldsymbol{x}),$$

where $\hat{z}$ is the estimated SOC, $\boldsymbol{x}$ is the present vector of input quantities for which an SOC estimate is desired, $\boldsymbol{x}_i$ for $1 \leqslant i \leqslant N$ is the vector i from the training dataset of total length N, α_i and α_i^* are tuning parameters, and $K(\boldsymbol{x}_i, \boldsymbol{x})$ is a "kernel function", which was chosen to be a quadratic function of the dot product $\boldsymbol{x}$ and $\boldsymbol{x}_i$ in this work. (Hu et al. and Antón et al. both use Gaussian kernel functions instead [41-42]).

Neural networks (NNs) comprise networks of interconnected simple processing elements that each compute some specific nonlinear function of a weighted combination of their inputs. Often, the hyperbolic tangent is selected as the nonlinear function. When the nonlinear function used by the network has a Gaussian form, the network is called a "radial basis function" (RBF) neural network. Taken altogether, these networks can be universal function approximators if sufficient "neurons" (processing elements) are included. The topology of the network must be designed and the weighting constants in each neuron must be tuned to be able to approximate an input–output relationship well. Some references that use neural networks to estimate SOC include [43-45]. ①

One vulnerability of all learning methods is the tendency to overfit the training data, essentially converging on a functional input–output relationship that fits the noise in the training data in addition to fitting the true underlying functional form of the input–output relationship. Special steps must be taken to improve the generalization ability of the trained networks such that they can produce reasonable estimates for field data that are different from training data. Chemali et al. [45], for example, combat this vulnerability by actually adding a low level of random noise to the training data to help make the predictions of the network more robust; i.e., they will make reasonable predictions of SOC in regions that are slightly perturbed from the input–output data used to train the network.

A second vulnerability of learning methods is that it is unclear how to account properly for cell aging. One possibility is to include in the training set samples from cells at all levels of expected aging, using lab-test accelerated-aging data. However,

① Neural networks have also been used to model the input-current to output-voltage dynamics of battery cells for use with various model-based estimators [46-47]. For example, Sun et al. in [48] used RBFs to model circuit component values in an equivalent-circuit model combined with an adaptive extended Kalman filter. These methods are fundamentally different in that they do not estimate SOC directly but instead contribute toward a cell model that can be used to estimate SOC using model-based approaches.

this approach is fundamentally flawed: it assumes that cell behaviors change in very repeatable ways as a cell ages. A critical reference [49] shows that this is not generally true, although it is routinely assumed to be true. If we cannot rely on lab-test accelerated-aging data, then we must rely on field data and these are very difficult to calibrate well. This issue must be overcome for learning methods to work robustly.

Proponents of learning methods sometimes claim that they are simpler than the model-based methods that we will study next. However, we need to evaluate this claim carefully: there is a difference between *conceptual* simplicity and *computational* simplicity. For someone well-versed in learning theory, SVMs and NNs may appear to be conceptually simpler than model-based methods. However, from the BMS designer's perspective, computational simplicity is far more important than conceptual simplicity, everything else being equal. That is, how many floating-point operations are required to produce a new SOC estimate having some level of quality? A method requiring as few floating-point operations as possible is preferred. Many SVM and NN-based methods require dozens or even hundreds of kernels/neurons to produce their outputs and can require significantly more computation than other methods.

2.3 Model-based estimation and dynamic cell models

One advantage of learning methods is that the BMS-algorithm designer requires no a priori knowledge of how battery cells work in order to implement an SOC estimator. However, proponents of model-based methods argue "don't estimate what you know already." That is, since there is already a body of knowledge on how to describe the operation of lithium-ion battery cells, there can be a huge benefit to incorporating that knowledge somehow into an estimator rather than using a black-box function approximator to attempt to learn that pre-existing knowledge in some generic format.

The methods that we will study in Sects. 2.4 and 2.5 rely on sets of mathematical equations ("models") that describe the input–output (current–voltage) dynamics of a battery cell. They incorporate those models into "model-based estimator" or "model-based observer" methods from different branches of control-systems theory that are designed to use models to estimate the internal state of a system.

The general approach is illustrated in Fig. 7. Electrical current is applied to or sourced by a physical battery cell, which changes the cell's SOC. However, we cannot measure the SOC directly; all we can measure are the electrical current and cell terminal voltage. So, we take the measured current and propagate it through a cell model. SOC is embedded in the model, so propagating current through the model modifies the variable in the model that represents SOC. The model further produces a predicted cell voltage. The predicted voltage and the measured voltage are compared and their difference is an indicator, in part, of how closely the model's SOC prediction matches the cell's actual SOC. Various types of feedback

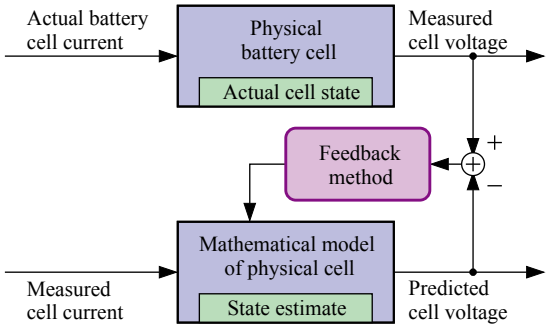

Figure 7 Principle of operation for model-based approaches (adapted from Fig. 1 in Ref. [36] and Fig. 3.5 in [98])

mechanism are used to convert the voltage-prediction error into a signal that adjusts the model state (including the SOC estimate). This SOC estimate is then the output of the model-based estimator.

A number of different kinds of model may be used with model-based estimators. We already noted in Footnote 1 that NNs can be used. However, the most popular type of model in use today for SOC estimation is the equivalent-circuit model (ECM). A fairly generic ECM is illustrated in Fig. 8. In the circuit, a dependent voltage source models the OCV versus SOC relationship; a nonlinear element models voltage hysteresis; the resistor R0 models the cell's equivalent series resistance (ESR); one or more parallel resistor–capacitor sub-circuits (e.g., R_1 in parallel with C_1)—themselves wired in series—model the slow time constants of lithium diffusion within the cell. Note that although a wide variety of ECM exist in the literature [50], they are all fundamentally similar, just with different elements included or excluded to adjust a balance between the complexity and fidelity of the model. For example, a circuit comprising only the voltage source and R_0 is commonly called the "Rint" model; a circuit further having a single parallel resistor–capacitor sub-circuit is called a Thévenin model; a circuit having instead two parallel resistor–capacitor sub-circuits is called a dual-RC model; the general circuit in Fig. 8 is called the "enhanced self-correcting" (ESC) cell model and includes all of the other named models as special cases in the Ref. [20-21, 38]. Additional generalizations of the circuit model can better describe cells having a blend of active materials in an electrode [51]; and constant-phase elements or Warburg impedances (modified capacitances requiring fractional-order calculus to implement [52])

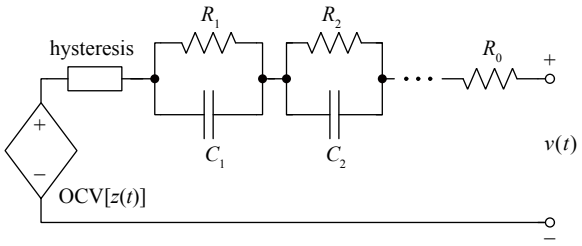

Figure 8 An equivalent-circuit model of a lithium-ion cell

can replace capacitors in the circuit to describe diffusion effects more directly, although a multiple resistor–capacitor circuit can approximate a constant-phase element or Warburg impedance very well.

ECMs can predict the input–output behaviors of a cell very well. However, they cannot describe internal electrochemical variables of the cell directly (i.e., the lithium concentrations and electrical potentials and rates of reaction at different locations internal to the cell). As discussed later, knowledge of these variables may be the key for future BMS to unlock untapped capabilities of lithium-ion cells, and so different kinds of models will be needed.

Specifically, so-called "physics-based models" (PBMs) will be required. Models in this category are derived from physical first principles of mass conservation and charge conservation and are most commonly stated as coupled sets of partial-differential equations (PDEs) [38-39]. The most popular is the Doyle–Fuller–Newman (DFN) porous-electrode pseudo-2d model [53]. The DFN model is generally considered to be too complex computationally to be used in BMS algorithms, so different approaches to simplifying the model have been proposed, and SOC estimators have been based on many of these simplifications. For example, single-particle models [54–58], enhanced single-particle models [59– 61], blend-electrode models [59, 61], and others [54–71].

2.4 Observer-based methods

To integrate either a learning model, ECM, or PBM with model-based estimators from the control-systems literature, the models must often be written in a very specific form: the discrete-time (nonlinear) state-space form,

$$\boldsymbol{x}_{k+1} = f(\boldsymbol{x}_k, u_k, w_k),$$

$$y_k = h(\boldsymbol{x}_k, u_k, v_k),$$

where $\boldsymbol{x}_k$ is a vector of values describing the state of the cell at time k, u_k is the input to the cell (in our case, the applied current: $u_k = i_{\text{app},k}$), w_k is process noise (an unmeasured input that can affect the state), y_k is the output (in our case, the terminal voltage), and v_k is unknown measurement noise. The state vector generally includes SOC as one of its components, so by computing an estimate $\hat{\boldsymbol{x}}_k$ of the true state $\boldsymbol{x}_k$ we compute at the same time an estimate of SOC. In an ECM, $\boldsymbol{x}_k$ also includes components describing the hysteresis state and the capacitor voltages (or resistor currents) in the resistor–capacitor sub-circuits. The state-equation function $f(\cdot,\cdot,\cdot)$ and measurement-equation function $h(\cdot,\cdot,\cdot)$ are chosen to model the input-to-state and state-to-output dynamics of the cell.

Observer-based methods commonly ignore the noises in the model equations (assuming $w_k = 0$ and $v_k = 0$) and comprise two steps: a first step predicts the present value of the state using prior information and the known state equation $f(\cdot,\cdot,\cdot)$; the second step updates the prediction using the present measured cell voltage and the known measurement equation $h(\cdot,\cdot,\cdot)$. The prediction might take the form

$$\hat{\boldsymbol{x}}_k^- = f(\hat{\boldsymbol{x}}_{k-1}^+, u_{k-1}, 0),$$

where the superscript "-" indicates a predicted quantity (uses only past information) and the superscript "+" indicates an estimated quantity (uses past and present information). We also predict the cell terminal voltage as

$$\hat{y}_k = h(\hat{\boldsymbol{x}}_k^-, u_k, 0),$$

and compute the state estimate as

$$\hat{\boldsymbol{x}}_k^+ = \hat{\boldsymbol{x}}_k^- + g(y_k - \hat{y}_k).$$

The specification of function $g(\cdot)$ distinguishes one kind of observer-based estimator from another. The simplest kind of estimator is the so-called Luenberger observer where

$$\hat{\boldsymbol{x}}_k^+ = \hat{\boldsymbol{x}}_k^- + \boldsymbol{L}(y_k - \hat{y}_k),$$

and $\boldsymbol{L}$ is a constant gain vector multiplying the voltage-prediction error; this method is used to estimate SOC in [22, 60, 68, 72-75]. A modification augments the proportional gain of the Luenberger observer with an integral term, resulting in a "proportional–integral (PI) observer", used to estimate SOC in [36].

Another class of observer-based estimator is known as a "sliding-mode observer". In this category, the feedback function $g(\cdot)$ is constrained to be of the form $\tilde{g}$ [sgn $(\cdot)$]; that is, only the sign of the prediction error is used, not the magnitude. Sliding-mode observers are known to be robust to modeling errors and guarantee that the model output will converge to the measured output in the absence of noise. SOC estimators using this technique are reported in [75-82]. A disadvantage of sliding-mode observers is that the estimate tends to "chatter" (have a large random error that switches between two limits). A modified sliding-mode observer is reported in [79] that reduces this chattering.

There are numerous other advanced observer-based methods applied to the SOC-estimation problem, including the backstepping method [55–58], a moving-horizon estimator [67], and a nonlinear fractional-order observer [75]. It is beyond the scope of this survey to describe the details of these methods, but the interested reader can confer the cited works, as well as the references that they themselves cite.

2.5 Adaptive-filter methods

In signal-processing theory, a *filter* is a method or system for estimating the true value of a signal that is somehow embedded in noisy measurements. In the SOC-estimation application, a history of noisy measurements of cell terminal voltage and cell electrical current must somehow be converted into an estimate of SOC. A common objective of adaptive-filter methods is to compute a state estimate that uses the entire history of observed data $\boldsymbol{Z}_k = \{u_0, u_1, \cdots, u_k, y_0, y_1, \cdots y_k\}$ to find the $\hat{\boldsymbol{x}}_k^+$ that minimizes the mean squared error with respect to the true state $\boldsymbol{x}_k$. That is, solve for

$$\hat{\boldsymbol{x}}_k^+ = \arg\min_{\hat{\boldsymbol{x}}\in\Re^n} \boldsymbol{E}\left[(\boldsymbol{x}_k - \hat{\boldsymbol{x}})^{\mathrm{T}}(\boldsymbol{x}_k - \hat{\boldsymbol{x}}) \,\middle|\, \boldsymbol{Z}_k\right]. \quad (4)$$

Adaptive-filter methods appear to have been applied first to the SOC-estimation problem for lead-acid cells [83–85]. They have subsequently been applied with great success to the SOC-estimation problem for lithium-ion cells.

Note that the solution to Eq. (4) can be shown to be $\hat{\boldsymbol{x}}_k^+ = \boldsymbol{E}[\boldsymbol{x}_k \,|\, \boldsymbol{Z}_k]$, but it is not possible to find a closed-form solution for this expression, in general. Different approaches are taken to approximate its value in general scenarios or to find exact solutions in specific scenarios. These are discussed in the next subsections.

Particle filters. Particle filters are the most general method to find an approximate solution to $\hat{\boldsymbol{x}}_k^+$. They are based on noticing that

$$\boldsymbol{E}[\boldsymbol{x}_k \,|\, \boldsymbol{Z}_k] = \int \boldsymbol{x}_k f(\boldsymbol{x}_k \,|\, \boldsymbol{Z}_k)\, \mathrm{d}\boldsymbol{x}_k,$$

where $f(\boldsymbol{x}_k \,|\, \boldsymbol{Z}_k)$ is the conditional probability density function (PDF) of $\boldsymbol{x}_k$ given $\boldsymbol{Z}_k$, and seeking to find ways to represent this PDF and compute the integral. The computation of the conditional PDF can, in principle, be divided into a prediction step

$$f(\boldsymbol{x}_k \,|\, \boldsymbol{Z}_{k-1}) = \int f(\boldsymbol{x}_k \,|\, \boldsymbol{x}_{k-1}) f(\boldsymbol{x}_{k-1} \,|\, \boldsymbol{Z}_{k-1})\, \mathrm{d}\boldsymbol{x}_{k-1},$$

and an update step

$$f(\boldsymbol{x}_k \,|\, \boldsymbol{Z}_k) = \frac{f(z_k \,|\, \boldsymbol{x}_k) f(\boldsymbol{x}_k \,|\, \boldsymbol{Z}_{k-1})}{f(z_k \,|\, \boldsymbol{Z}_{k-1})},$$

as illustrated in Fig. 9.

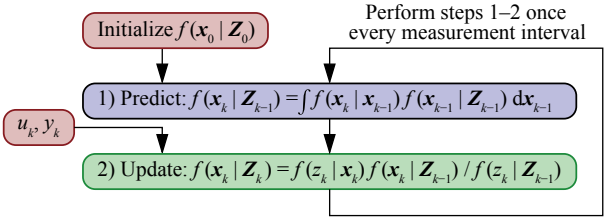

Figure 9 The particle-filter method

Except in trivial cases, there is no known solution to the integral, so its value must be evaluated numerically, which is exceptionally demanding computationally due to the high dimensionality of the state vector $\boldsymbol{x}_k$. Particle filters reduce the required computation by approximating the integral using Monte-Carlo methods [86]. Another challenge relates to how to store the conditional PDFs that are propagated from one timestep to the next. Particle filters overcome this obstacle by storing sets of random samples (the "particles") from the PDFs such that the set of particles collectively describes the PDFs much like a histogram of data samples can describe a PDF. In order to make good approximations, many particles are needed, and so particle-filter methods generally have very high computational complexity. For this reason, particle filters are often considered a "last resort" estimation method, but they can also provide very-high-quality near-optimal state estimates. Particle filters are used to estimate SOC in [23, 61, 87-91].

2.5.1 Kalman-filter methods, in general

Kalman filters of different varieties (xKFs) take a very different approach from particle filters to finding $\boldsymbol{E}[\boldsymbol{x}_k \,|\, \boldsymbol{Z}_k]$. Instead of attempting either to find or approximate the optimal solution in a general sense, they reduce the permitted generality by placing assumptions on the PDFs of all random variables in the problem: xKFs assume that the process noise w_k and the sensor noise v_k are mutually uncorrelated white Gaussian noise processes, and that the uncertain state $\boldsymbol{x}_k$ also has a Gaussian distribution. Generically, $\boldsymbol{E}[\boldsymbol{x}_k \,|\, \boldsymbol{Z}_k]$ can be divided into two steps: a prediction step and an update step,

$$\hat{\boldsymbol{x}}_k^- = \boldsymbol{E}[\boldsymbol{x}_k \,|\, \boldsymbol{Z}_{k-1}],$$

$$\hat{\boldsymbol{x}}_k^+ = \hat{\boldsymbol{x}}_k^- + \boldsymbol{E}[(\boldsymbol{x}_k - \hat{\boldsymbol{x}}_k^-) \,|\, \{u_k, y_k\}].$$

Under the Gaussian assumption, the conditional expectation in the update step can be written as

$$\hat{\boldsymbol{x}}_k^+ = \hat{\boldsymbol{x}}_k^- + \underbrace{\boldsymbol{\Sigma}_{\tilde{x}\tilde{y},k}^- \boldsymbol{\Sigma}_{\tilde{y},k}^{-1}}_{\boldsymbol{L}_k} (y_k - \hat{y}_k),$$

where $\boldsymbol{L}_k$ is the time-varying optimal filter gain, $\boldsymbol{\Sigma}_{\tilde{y},k} = \boldsymbol{E}\left[(y_k - \hat{y}_k)(y_k - \hat{y}_k)^{\mathrm{T}}\right]$ is the covariance matrix of the output prediction error and describes the uncertainty of the prediction, and $\boldsymbol{\Sigma}_{\tilde{x}\tilde{y},k}^- = \boldsymbol{E}\left[\left(\boldsymbol{x}_k - \hat{\boldsymbol{x}}_k^-\right)(y_k - \hat{y}_k)^{\mathrm{T}}\right]$ is the cross-covariance matrix between the state prediction error and the output prediction error and jointly describes the uncertainty of the state prediction and its connection to the output prediction error.

It is possible to come up with a sequence of two major steps—each having three substeps—to evaluate the terms in these equations, as illustrated in Fig. 10 and itemized below. (For

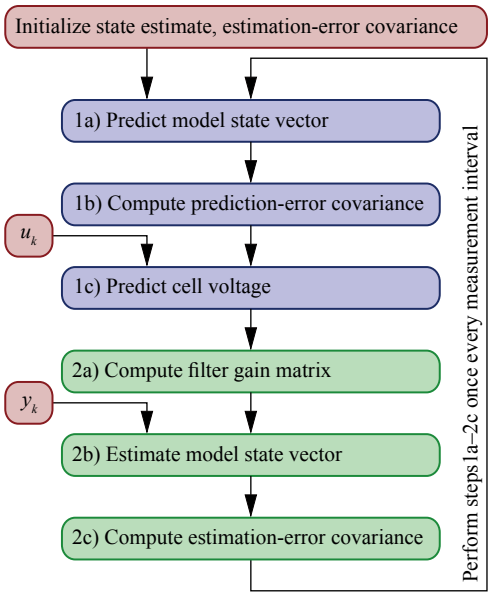

Figure 10 The generic steps shared by all xKFs

more details on deriving the equations, see for example references [92-96]).

1a) Predict model state vector: $\hat{\boldsymbol{x}}_k^- = \boldsymbol{E}[\boldsymbol{x}_k \mid \boldsymbol{Z}_{k-1}]$.

1b) Compute prediction-error covariance: $\boldsymbol{\Sigma}_{\tilde{x},k}^- = \boldsymbol{E}[(\boldsymbol{x}_k - \hat{\boldsymbol{x}}_k^-)(\boldsymbol{x}_k - \hat{\boldsymbol{x}}_k^-)^{\mathrm{T}}]$.

1c) Predict cell voltage: $\hat{y}_k = \boldsymbol{E}[y_k \mid \boldsymbol{Z}_{k-1}]$.

2a) Compute filter gain matrix: $\boldsymbol{L}_k = \boldsymbol{E}[(\boldsymbol{x}_k - \hat{\boldsymbol{x}}_k^-)(y_k - \hat{y}_k)^{\mathrm{T}}]\boldsymbol{E}[(y_k - \hat{y}_k)(y_k - \hat{y}_k)^{\mathrm{T}}]^{-1}$.

2b) Estimate model state vector: $\hat{\boldsymbol{x}}_k^+ = \boldsymbol{E}[\boldsymbol{x}_k \mid \boldsymbol{Z}_k]$.

2c) Compute estimation-error covariance: $\boldsymbol{\Sigma}_{\tilde{x},k}^+ = \boldsymbol{E}[(\boldsymbol{x}_k - \hat{\boldsymbol{x}}_k^+)(\boldsymbol{x}_k - \hat{\boldsymbol{x}}_k^+)^{\mathrm{T}}]$.

First, we predict the model state using prior measurements; second, we compute the covariance matrix of the state-prediction error (describing the uncertainty of the state prediction versus the true but unknown state); third, we predict the cell voltage; fourth, we compute the filter gain matrix $\boldsymbol{L}_k$; fifth, we compute the state estimate $\hat{\boldsymbol{x}}_k^+$; finally, we compute the state-estimation-error covariance matrix (describing the uncertainty of the state estimate). Overall, the solution comprises a set of computationally efficient recursive relationships that produces as its output at every time step k both an estimate of the state itself $\hat{\boldsymbol{x}}_k^+$ and also the covariance matrix $\boldsymbol{\Sigma}_{\tilde{x},k}^+$ of the state-estimation error. The covariance matrix indicates the uncertainty of the state estimate and may be used to generate confidence bounds on the estimate. A "large" $\boldsymbol{\Sigma}_{\tilde{x},k}$ (one with large singular values) indicates a high level of uncertainty in the state estimate; a "small" $\boldsymbol{\Sigma}_{\tilde{x},k}$ (one with small singular values) indicates high confidence in the accuracy of the estimate.

2.5.2 The linear Kalman filter (KF)

We still require methods to evaluate the statistical expectations in steps 1a–2c. The linear Kalman filter accomplishes this goal by further assuming that the system whose state is being estimated can be written in a linear discrete-time state-space form:

$$\boldsymbol{x}_{k+1} = \boldsymbol{A}_k \boldsymbol{x}_k + \boldsymbol{B}_k u_k + w_k ,$$

$$\boldsymbol{y}_k = \boldsymbol{C}_k \boldsymbol{x}_k + \boldsymbol{D}_k u_k + v_k ,$$

where $\boldsymbol{A}_k$, $\boldsymbol{B}_k$, $\boldsymbol{C}_k$, and $\boldsymbol{D}_k$ are (possibly time-varying) matrices containing the constants required to model the system dynamics. Under these assumptions, we derive the standard linear Kalman filter whose steps are summarized in Table. 1. Researchers have reported using KF to estimate SOC in [46, 63-64, 83-84], and a fractional-order version in [97].

2.5.3 The extended Kalman filter (EKF)

Under the assumptions made in its derivation, the Kalman filter is the optimal (minimum mean squared error) state estimator for linear systems. Nonlinear systems have dynamics that can also often be expressed in a state-space form:

$$\boldsymbol{x}_{k+1} = f(\boldsymbol{x}_k, u_k) + w_k ,$$

$$\boldsymbol{y}_k = g(\boldsymbol{x}_k, u_k) + v_k ,$$

where $f(\cdot,\cdot)$ and $g(\cdot,\cdot)$ are nonlinear functions that describe the state dynamics and measurement. For nonlinear systems, there is no general solution for the optimal filter. Instead, assumptions and approximations are usually made to generalize

Table 1 Summary of the linear Kalman filter from reference [95]

Linear state-space model:

$$x_{k+1} = A_k x_k + B_k u_k + w_k,$$

$$y_k = C_k x_k + D_k u_k + v_k.$$

where w_k and v_k are independent, zero-mean, Gaussian noise processes of covariance matrices $\boldsymbol{\Sigma}_{\tilde{w}}$ and $\boldsymbol{\Sigma}_{\tilde{v}}$, respectively.

Initialization: For $k = 0$, set

$$\hat{x}_0^+ = \boldsymbol{E}[x_0]$$

$$\boldsymbol{\Sigma}_{\tilde{x},0}^+ = \boldsymbol{E}[(x_0 - \hat{x}_0^+)(x_0 - \hat{x}_0^+)^{\mathrm{T}}].$$

Computation: For $k = 1, 2, \ldots$ compute:

Predict model state vector:	$\hat{x}_k^- = A_{k-1}\hat{x}_{k-1}^+ + B_{k-1}u_{k-1}.$
Compute prediction-error covariance:	$\boldsymbol{\Sigma}_{\tilde{x},k}^- = A_{k-1}\boldsymbol{\Sigma}_{\tilde{x},k-1}^+ A_{k-1}^{\mathrm{T}} + \boldsymbol{\Sigma}_{\tilde{w}}.$
Predict cell voltage:	$\hat{y}_k = C_k\hat{x}_k^- + D_k u_k.$
Compute filter gain matrix:	$L_k = \boldsymbol{\Sigma}_{\tilde{x},k}^- C_k^T [C_k \boldsymbol{\Sigma}_{\tilde{x},k}^- C_k^{\mathrm{T}} + \boldsymbol{\Sigma}_{\tilde{v}}]^{-1}.$
Estimate model state vector:	$\hat{x}_k^+ = \hat{x}_k^- + L_k (y_k - \hat{y}_k).$
Compute estimation-error covariance:	$\boldsymbol{\Sigma}_{\tilde{x},k}^+ = (I - L_k C_k)\boldsymbol{\Sigma}_{\tilde{x},k}^-.$

the linear Kalman filter to nonlinear systems. The extended Kalman filter (EKF) is the most popular such generalization, which makes two fundamental assumptions in its derivation:

1) In computing state estimates, EKF assumes $\boldsymbol{E}[\text{fn}(x)] \approx \text{fn}(\boldsymbol{E}[x])$, which is true only for linear systems and can be far from true for highly nonlinear systems;

2) In computing covariance estimates, EKF linearizes the nonlinear model around the present operating point using Taylor series, losing accuracy for highly nonlinear systems.

The net effect of these assumptions is that the EKF tends to work well for systems having mild nonlinearities and not as well for systems having strong nonlinearities. The overall EKF algorithm is summarized in Table 2 and is applied to the SOC-estimation problem in [98-99].

Lithium-ion battery cells tend to have quite linear dynamics at warm temperatures (LFP cells can be an exception, having significant nonlinear hysteresis even at warm temperatures). Therefore, EKF can be a good state estimator for BMS applications. An example of EKF state estimation is shown in Fig. 11, where the experiment applied a sequence of urban dynamometer driving schedule (UDDS) profiles to the cell over its entire SOC range. The left frame shows a cell's true SOC versus time as a thick black line, the EKF's estimate of SOC as the thick blue line, and the confidence bounds produced by the EKF (three-sigma bounds, computed from the covariance matrix $\boldsymbol{\Sigma}^{+}_{\tilde{x},k}$) as thin blue lines. We can see that the estimate tracks the true SOC closely. This is perhaps easier to see in the right frame of the figure, which plots the estimation error $\boldsymbol{x}_k - \hat{\boldsymbol{x}}_k$ instead, along with estimation-error bounds. We desire that this error be close to zero and that the bounds always encompass the error, which in this case they do. This level of SOC-estimation error is typical for EKF using highly calibrated data and relatively noise-free sensors such as when using laboratory data for lithium-ion chemistries different from LFP. Using a practical BMS measurement system having less precise sensors and less careful synchronization between voltage and current measurements, we would expect SOC estimation error to be higher. And, for LFP, we would also expect SOC estimation error to be higher due to difficult-to-model hysteresis and the flatness of the OCV versus SOC relationship, which dilutes the information present in a cell voltage measurement.

EKF is perhaps the most common adaptive-filtering approach to SOC estimation [20-21, 26, 46, 54, 59, 61-62, 66, 69-71, 73, 85, 87, 90, 100-113]. Researchers have also proposed modifications to the basic approach, including adaptive fading EKF [105], fractional-order EKF [114], iterated EKF [115], multi-model EKF [105], and robust EKF [103, 116].

2.5.4 Adaptive EKF (AEKF)

When implementing a Kalman-filtering SOC estimator, the BMS algorithm designer must define several tuning variables to adjust the performance of the filter to be acceptable under all operating conditions. These include: the covariance of the

Table 2 Summary of the nonlinear extended Kalman filter from reference [100]

Nonlinear state-space model:

$$x_{k+1} = f(x_k, u_k) + w_k,$$
$$y_k = g(x_k, u_k) + v_k.$$

where w_k and v_k are independent, zero-mean, Gaussian noise processes of covariance matrices $\boldsymbol{\Sigma}_{\tilde{w}}$ and $\boldsymbol{\Sigma}_{\tilde{v}}$, respectively.

Definitions:

$$\hat{A}_k = \left.\frac{\partial f(x_k,u_k)}{\partial x_k}\right|_{x_k=\hat{x}_k^+} \qquad \hat{C}_k = \left.\frac{\partial g(x_k,u_k)}{\partial x_k}\right|_{x_k=\hat{x}_k^-}.$$

Initialization: For $k = 0$, set

$$\hat{x}_0^+ = \boldsymbol{E}[x_0]$$
$$\boldsymbol{\Sigma}^+_{\tilde{x},0} = \boldsymbol{E}[(x_0 - \hat{x}_0^+)(x_0 - \hat{x}_0^+)^{\mathrm{T}}].$$

Computation: For $k = 1, 2, \ldots$ compute:

Predict model state vector: $\hat{x}_k^- = f(\hat{x}_{k-1}^+, u_{k-1}).$

Compute prediction-error covariance: $\boldsymbol{\Sigma}^-_{\tilde{x},k} = \hat{A}_{k-1}\boldsymbol{\Sigma}^+_{\tilde{x},k-1}\hat{A}^{\mathrm{T}}_{k-1} + \boldsymbol{\Sigma}_{\tilde{w}}.$

Predict cell voltage: $\hat{y}_k = g(\hat{x}_k^-, u_k).$

Compute filter gain matrix: $L_k = \boldsymbol{\Sigma}^-_{\tilde{x},k}\hat{C}_k^{\mathrm{T}}[\hat{C}_k\boldsymbol{\Sigma}^-_{\tilde{x},k}\hat{C}_k^{\mathrm{T}} + \boldsymbol{\Sigma}_{\tilde{v}}]^{-1}.$

Estimate model state vector: $\hat{x}_k^+ = \hat{x}_k^- + L_k(y_k - \hat{y}_k).$

Compute estimation-error covariance: $\boldsymbol{\Sigma}^+_{\tilde{x},k} = (I - L_k\hat{C}_k)\boldsymbol{\Sigma}^-_{\tilde{x},k}.$

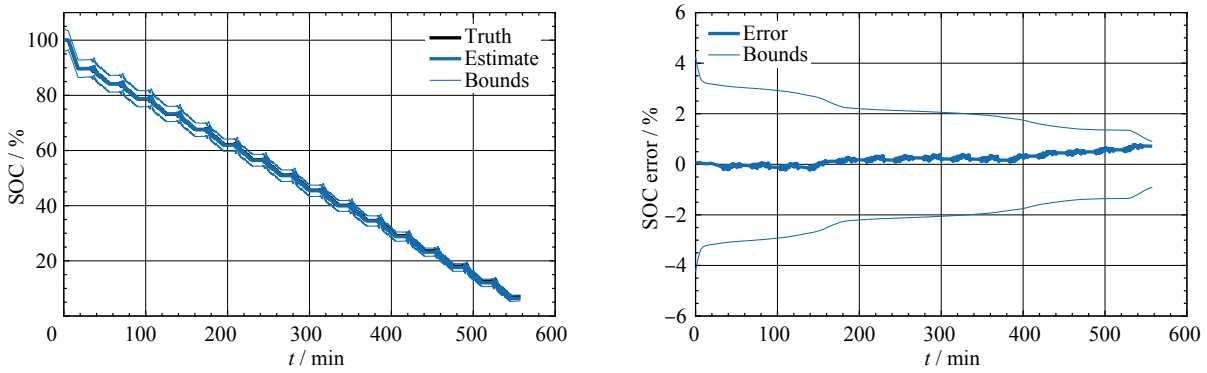

(a) SOC estimation using EKF (b) SOC estimation errors using EKF

Figure 11 An example of SOC estimation using EKF

initial state estimate $\boldsymbol{\Sigma}^{+}_{\tilde{x},0}$, the covariance matrix of the process noise $\boldsymbol{\Sigma}_{\tilde{w}}$, and the covariance matrix of the sensor noise $\boldsymbol{\Sigma}_{\tilde{v}}$. These covariances are not generally possible to derive analytically, and often a trial-and-error approach is taken to find matrices that cause the xKF to work well.

An alternative is to modify somewhat the xKF equations such that the process-noise and/or the sensor-noise covariances are adapted over time along with the state estimate. Care must be taken to ensure that this adaptive process is stable, but researchers have reported very good SOC-estimation results using adaptive EKF, for example [14, 47-48, 117-120].

2.5.5 The sigma-point Kalman filter (SPKF/UKF/CKF)

For strongly nonlinear systems, the EKF can fail, requiring stronger estimation methods: in those cases, the sigma-point approach is often preferred. In this approach,

1) Derivatives do not need to be computed (which is one of the most error-prone steps when implementing EKF), also implying

2) The original functions do not need to be differentiable, and

3) Better covariance approximations are usually achieved, relative to EKF, allowing for better and more reliable state estimation.

The sigma-point approach is *conceptually* more complex than the EKF but its *computational complexity* is identical to the EKF, so there is little reason not to use it in a BMS.

The derivation of the sigma-point Kalman filter (SPKF) differs from EKF in how it evaluates the statistics at the output of a nonlinear function when the input is a random variable. Instead of linearizing the function and using Taylor series, a sequence of function evaluations is performed using samples from the input random variable, and statistics of the function outputs are computed to find the desired expectations and covariances. Specifically, a set of sigma points $\boldsymbol{\mathcal{X}}$ is chosen so that the (possibly weighted) mean and covariance of the points exactly matches the mean $\bar{x}$ and covariance $\boldsymbol{\Sigma}_{\tilde{x}}$ of the input random variable being modeled. These points are then passed through the nonlinear function, resulting in a transformed set of points $\boldsymbol{\mathcal{Y}}$. The mean $\bar{y}$ and covariance $\boldsymbol{\Sigma}_{\tilde{y}}$ of the function-output random variable are then approximated by the mean and covariance of these transformed points $\boldsymbol{\mathcal{Y}}$.

Note that the sigma points comprise a fixed small number of vectors that are calculated deterministically—not like particle-filter methods. If the input random variable x has dimension L, mean $\bar{x}$, and covariance $\boldsymbol{\Sigma}_{\tilde{x}}$, then $p+1 = 2L+1$ sigma points are generated as the set

$$\mathcal{X} = \{\bar{x}, \bar{x} + \gamma\sqrt{\boldsymbol{\Sigma}_{\tilde{x}}}, \bar{x} - \gamma\sqrt{\boldsymbol{\Sigma}_{\tilde{x}}}\}, \tag{5}$$

with members of $\boldsymbol{\mathcal{X}}$ indexed from 0 to p, and where the matrix square root $\boldsymbol{R} = \sqrt{\boldsymbol{\Sigma}}$ computes a result such that $\boldsymbol{\Sigma}=\boldsymbol{R}\boldsymbol{R}^{\mathrm{T}}$ (e.g., using the Cholesky decomposition). These sigma points are passed through the nonlinear function one at a time to produce the output set of sigma points $\boldsymbol{\mathcal{Y}}$. The weighted mean and covariance of $\boldsymbol{\mathcal{Y}}$ are computed as

$$\bar{y} = \sum_{i=0}^{p} \alpha_i^{(\mathrm{m})} \boldsymbol{\mathcal{Y}}_i \text{ and } \boldsymbol{\Sigma}_{\tilde{y}} = \sum_{i=0}^{p} \alpha_i^{(\mathrm{c})} (\boldsymbol{\mathcal{Y}}_i - \bar{y})(\boldsymbol{\mathcal{Y}}_i - \bar{y})^{\mathrm{T}},$$

where $\boldsymbol{\mathcal{Y}}_i$ is the ith member of $\boldsymbol{\mathcal{Y}}$, and both $\alpha_i^{(\mathrm{m})}$ and $\alpha_i^{(\mathrm{c})}$ are real scalars.

There are different families of SPKFs, which are distinguished only by the sets of weighting factors $\{\gamma, \alpha_i^{(\mathrm{m})}, \alpha_i^{(\mathrm{c})}\}$ chosen in the implementation. The central-difference Kalman filter, unscented Kalman filter, and cubature Kalman filter are all types of SPKF and do not differ from each other in fundamental ways from a practical point of view.

The overall SPKF algorithm is summarized in Table 3 and is applied to the SOC-estimation problem in Ref. [98-99], where the somewhat nonstandard mathematical notation of Eq. (5) is also explained in detail. Researchers have reported using SPKF to estimate SOC in [73, 113, 121-122], the specific UKF variant in [17, 65, 87, 90, 110, 112, 123-129], a strong-tracking SPKF variation (designed to improve covariance estimates) in [130], and a fractional-order UKF version in [131].

2.5.6 Recursive least squares

Kalman filters are designed to find estimates of the state of a

Table 3 Summary of the nonlinear sigma-point Kalman filter from reference [122]

Nonlinear state-space model:

$$x_k = f(x_{k-1}, u_{k-1}, w_{k-1}, k-1)$$

$$y_k = h(x_k, u_k, v_k, k),$$

where w_k and v_k are independent, Gaussian noise processes of covariance matrices $\boldsymbol{\Sigma}_{\tilde{w}}$ and $\boldsymbol{\Sigma}_{\tilde{v}}$, respectively.

Definitions: Let

$$x_k^a = [x_k^{\mathrm{T}},\ w_k^{\mathrm{T}},\ v_k^{\mathrm{T}}]^{\mathrm{T}}, \quad \mathcal{X}_k^a = [(\mathcal{X}_k^x)^{\mathrm{T}},\ (\mathcal{X}_k^w)^{\mathrm{T}},\ (\mathcal{X}_k^v)^{\mathrm{T}}]^{\mathrm{T}}, \quad p = 2 \times \dim(x_k^a).$$

Initialization: For $k = 0$, set

$$\hat{x}_0^+ = \boldsymbol{E}[x_0] \qquad \hat{x}_0^{a,+} = \boldsymbol{E}[x_0^a] = [(\hat{x}_0^+)^{\mathrm{T}},\ \bar{w},\ \bar{v}]^{\mathrm{T}}.$$

$$\boldsymbol{\Sigma}_{\tilde{x},0}^+ = \boldsymbol{E}[(x_0 - \hat{x}_0^+)(x_0 - \hat{x}_0^+)^{\mathrm{T}}] \qquad \boldsymbol{\Sigma}_{\tilde{x},0}^{a,+} = \boldsymbol{E}[(x_0^a - \hat{x}_0^{a,+})(x_0^a - \hat{x}_0^{a,+})^{\mathrm{T}}]$$

$$= \mathrm{diag}(\boldsymbol{\Sigma}_{\tilde{x},0}^+, \boldsymbol{\Sigma}_{\tilde{w}}, \boldsymbol{\Sigma}_{\tilde{v}}).$$

Computation: For $k = 1, 2, \ldots$ compute:

Predict model state vector:

$$\mathcal{X}_{k-1}^{a,+} = \left\{\hat{x}_{k-1}^{a,+},\ \hat{x}_{k-1}^{a,+} + \gamma\sqrt{\boldsymbol{\Sigma}_{\tilde{x},k-1}^{a,+}},\ \hat{x}_{k-1}^{a,+} - \gamma\sqrt{\boldsymbol{\Sigma}_{\tilde{x},k-1}^{a,+}}\right\}.$$

$$\mathcal{X}_{k,i}^{x,-} = f(\mathcal{X}_{k-1,i}^{x,+}, u_{k-1}, \mathcal{X}_{k-1,i}^{w,+}, k-1).$$

$$\hat{x}_k^- = \sum_{i=0}^{p} \alpha_i^{(\mathrm{m})} \mathcal{X}_{k,i}^{x,-}.$$

Compute prediction-error covariance:

$$\boldsymbol{\Sigma}_{\tilde{x},k}^- = \sum_{i=0}^{p} \alpha_i^{(\mathrm{c})} (\mathcal{X}_{k,i}^{x,-} - \hat{x}_k^-)(\mathcal{X}_{k,i}^{x,-} - \hat{x}_k^-)^{\mathrm{T}}.$$

Predict cell voltage:

$$\mathcal{Y}_{k,i} = h(\mathcal{X}_{k,i}^{x,-}, u_k, \mathcal{X}_{k-1,i}^{v,+}, k).$$

$$\hat{y}_k = \sum_{i=0}^{p} \alpha_i^{(\mathrm{m})} \mathcal{Y}_{k,i}.$$

Compute filter gain matrix:

$$\boldsymbol{\Sigma}_{\tilde{y},k} = \sum_{i=0}^{p} \alpha_i^{(\mathrm{c})} (\mathcal{Y}_{k,i} - \hat{y}_k)(\mathcal{Y}_{k,i} - \hat{y}_k)^{\mathrm{T}}.$$

$$\boldsymbol{\Sigma}_{\tilde{x}\tilde{y},k}^- = \sum_{i=0}^{p} \alpha_i^{(\mathrm{c})} (\mathcal{X}_{k,i}^{x,-} - \hat{x}_k^-)(\mathcal{Y}_{k,i} - \hat{y}_k)^{\mathrm{T}}.$$

$$L_k = \boldsymbol{\Sigma}_{\tilde{x}\tilde{y},k}^- \boldsymbol{\Sigma}_{\tilde{y},k}^{-1}.$$

Estimate model state vector:

$$\hat{x}_k^+ = \hat{x}_k^- + L_k(y_k - \hat{y}_k).$$

Compute estimation-error covariance:

$$\boldsymbol{\Sigma}_{\tilde{x},k}^+ = \boldsymbol{\Sigma}_{\tilde{x},k}^- - L_k \boldsymbol{\Sigma}_{\tilde{y},k} L_k^{\mathrm{T}}.$$

dynamic system by minimizing a mean-squared cost function. Recursive least squares (RLS) attempts to minimize a least-squares cost function, but the application is to determining a constant unknown vector using deterministic inputs and not a dynamic vector using stochastic inputs. Since the state of a battery cell model is not a constant (e.g., SOC varies with time) and since there are random noises on the measurements of current and voltage, there is no theoretic justification to applying RLS to the SOC-estimation problem. However, by slightly modifying RLS to add "forgetting factors" some researchers have shown that RLS can still provide good SOC estimates in some cases. Examples include in the Ref. [15, 120].

2.5.7 Others

There are other adaptive-filter approaches to estimating battery-cell SOC. For example, instead of attempting to minimize a mean-squared cost function, it is possible to minimize a worst-case-error cost function. Technically, instead of minimizing a H_2 norm, this would be minimizing a H_∞ norm. Adaptive filters that minimize this norm are called H_∞ observers, and some researchers have applied them to SOC estimation [132–134]. Other less-common adaptive-filter methods applied to SOC estimation include Kalman smoothers [61] and nonlinear predictive filters [135].

3 Cell state of charge versus pack state of charge

Until this point, we have focused on methods to estimate the SOC of a single battery cell. We now consider the needs of SOC estimation for a battery pack, comprising many cells wired in parallel and/or in series. Battery-pack SOC estimation is considered in the Ref. [12, 16, 48, 72, 109-111, 113, 118, 127, 129, 135].

First, consider multiple cells wired in parallel. By Kirchhoff's voltage law, they must have identical terminal voltages. Due to expense, it is uncommon to measure individual cell current (usually, only battery-pack current is measured), so it is impossible to distinguish one cell's SOC from another's. This is not a large concern because, even if SOCs differ from one another in a transient sense, the common terminal voltage will cause SOCs to converge whenever the pack rests (and tend to stay close even when the pack is active). Thus, to estimate the average SOC of N_p parallel-connected cells, the measured pack current is divided by N_p and provided to any of the previously seen SOC estimation methods along with the voltage of the

connected cells. From now on, we consider cells wired in parallel as a single logical cell.

Estimating SOC for cells wired in series requires more thought. For many applications, it would be advantageous to define a single "battery-pack SOC" metric that could be used by all BMS functions rather than needing to compute and interpret individual SOC estimates for every one of the series-connected cells.

Figure 12 attempts to illustrate the logical fallacy of this approach. In this trivial two-cell battery pack, one cell has SOC of 0% and the other has SOC of 100%. How should we define battery-pack SOC for this case? Should it be 0% because we cannot discharge the pack without overdischarging the lower cell? That would be misleading because defining a battery pack SOC of 0% gives the impression that we can charge the pack, and in this case we cannot do so without overcharging the upper cell.

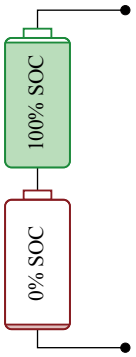

Figure 12 Illustrating the logical fallacy of "battery-pack SOC".

So, should the battery-pack SOC be defined to be 100%? That is also misleading because it leads us to think that we can discharge the pack, which we cannot without over-discharging the lower cell. How about the average of the two, 50%? That is also misleading because it leads us to think that we can both discharge and charge the pack, which we cannot.

This mental exercise shows us the value of SOE estimates, which for this example would return 0Wh because we cannot withdraw energy from the pack. It also shows the value of SOF/SOP estimates, which in this case would be 0W charge power and 0W discharge power. SOC should not be used as a fuel gauge by itself (SOE is usually what is wanted). This exercise also shows us the folly of attempting to define a battery-pack SOC metric. There is no physical significance to battery-pack SOC; there is physical significance only to cell SOC, as we saw earlier. Some researchers attempt to define a battery-pack SOC for "reasonably-well balanced" packs, but these are engineering SOC definitions, not physical SOC definitions. This kind of engineering pack SOC definition will ultimately suffer from many of the same problems as ESOC applied to single cells.

But, that leaves us with a serious problem: if a battery pack connects N_s cells in series, do we need to estimate N_s individual SOC values? Yes. But, a few observations show that the computational complexity of doing so does not need to be significantly larger than running a single SOC estimator for a single cell.

Bar-delta filtering. The first reference of which we are aware to estimate SOC efficiently for all cells in a battery pack was termed "bar delta filtering" [98, 113]. In this approach, one filter estimated the pack-average state and N_s additional filters estimated the differences between individual cell states and the pack-average state. The pack-average filter was named the "bar" filter since the mean of a variable is often represented with an overbar (e.g., $\bar{x}$) and the difference filters were named the "delta" filters since deviations are often represented using the delta symbol (e.g., Δx).

At first, it appears that this has taken a problem of computational complexity N_s (implementing N_s independent SOC estimators, each having some required number of operations) and replaced it with a problem of complexity N_s+1 (implementing N_s+1 estimators). However, this is not the case for two reasons: 1) the delta filters have far lower computational complexity than the full state estimator, and 2) the delta filters can be executed at a reduced update rate.

The full state estimator for a single cell must estimate the cell's SOC along with other model states that might include hysteresis and multiple capacitor voltages if using an ECM. The "bar" filter must estimate the same number of quantities (i.e., the averages of all cell SOCs, hysteresis states, and capacitor voltages) and so has the same computational complexity as a single-cell SOC estimator. However, the "delta" filters need only estimate the difference between a particular cell's SOC and the pack-average SOC, so need have only a single state. The computational complexity of the individual "delta" filters is thus reduced.

The full state estimator for a single cell must have an update rate that is fast enough to capture the dynamics of the cell. The same is true of the "bar" filter. However, while an individual cell's SOC might change quickly, the difference between a cell's SOC and the pack-average SOC changes very slowly, caused by small differences in capacity between cells in the battery pack. Therefore, the "delta" filters do not need to be updated at the same rate as the "bar" filter. In the limit, we might update only one "delta" filter per iteration of the "bar" filter, resulting in a computational complexity for the entire algorithm of only slightly more than the computational complexity of a single-cell SOC estimator.

Cell mean model plus cell difference model. More recently, Zheng et al. have proposed a somewhat different method for estimating SOC of all cells in a battery pack [16, 109]. Similar to the bar-delta approach, a cell-mean model (CMM) is used to estimate a pack-average state and a cell-difference model is used to estimate the differences between the pack-average and individual cell states. However, the cell-difference models are constrained to be of a simplified "Rint" form, and instead

of estimating a difference in SOC directly, these authors first estimate a difference in OCV between individual cells and the pack average. Then, the difference in OCV is related to a difference in SOC. Studying the details of this approach uncovers a significant advantage over the previous bar-delta method: precise estimates of individual cell capacities are no longer needed (which are very difficult to estimate accurately in practice even using the best methods)—all that is needed is an estimate of cell resistance, which is far easier to estimate since it is a far more observable parameter in the model. Similar to bar-delta, the CMM+CDM method can operate on two timescales and the cell-difference states are very quickly computed, giving reduced computational complexity of a similar level. In sum, using this method can provide accurate estimates of all SOCs in a series-connected battery pack at a very reasonable level of computation.

4 Discussion and perspectives on the field

4.1 How to select an estimator

As we approach the end of this article, I would like to highlight a few perspectives on the field. We have now reviewed a number of general methodologies for estimating SOC, but the algorithm designer ultimately needs to make a choice regarding which one to implement. How to make this choice?

From a technical perspective, the choice is dictated by the requirements of the application. How much computational power is available? How must the estimator respond as the cell ages? For what purpose is the SOC estimate being used? How accurate must the SOC estimate be?

In terms of computational power, we have already discussed the distinction between computational complexity—which is an objective measure—and conceptual complexity—which is a subjective measure. I propose that it is more important that an algorithm be computationally simple (enabling less-expensive microcontroller and electronics) than that it be conceptually simple. Indeed, even an algorithm that is difficult to understand at first becomes familiar after some experience.

In terms of aging, the learning-based methods are at a disadvantage. For them to work well, training data must be collected from cells operating in all possible (both likely and unlikely) aged states and used to tune the parameter values of the estimator. Model-based approaches have the advantage that a suitably designed ECM or PBM has enough flexibility in its equations to describe the dynamics of a lithium-ion battery cell at all possible states of life if the parameters of the model can be adjusted by the BMS to match the cell at that state of life (this is another topic entirely, sometimes termed "state-of-health estimation", but is in fact more general than that, and it is beyond the scope of this survey paper).

The purpose for which the SOC estimate is required is also a primary consideration. For example, by combining SOC with a known total capacity and OCV versus SOC relationship, it is possible to compute the *total residual energy* in a cell [98]. However, computing *available energy* before encountering a minimum-voltage cutoff further requires knowledge of the entire cell state (e.g., hysteresis value and capacitor voltages in an ECM). Similarly, accurate computation of available power requires knowledge of the full cell state [98, 136]. Model-based approaches automatically provide estimates of the entire cell state, producing improved SOE and SOP estimates. Adaptive-filter-based approaches further produce confidence bounds on the estimate at no additional computational cost, which is critical for computing robust and actionable follow-on estimates of SOE, SOP, and so forth. For this reason, I prefer adaptive-filter methods.

In terms of SOC-estimation accuracy for the adaptive-filter methods, particle filters can produce the most-accurate estimates, followed by SPKF (including UKF and CKF variants), followed by EKF, and finally by KF. However, the accuracy of the SOC estimates produced by any given implementation depends directly on the accuracy of the model being used as much as or even more than it depends on the type of adaptive filter being used. Many authors have reported on the importance of using a good model [17, 81, 108, 114, 116, 119], and some have specifically commented on the importance of a good OCV versus SOC relationship in the model [123, 137]. SOC estimation for iron-phosphate LFP cells is especially difficult due to the high levels of hysteresis present and the flatness of the OCV versus SOC relationship: some authors who have reported SOC-estimation results for LFP cells include [14-17, 22-24, 26, 41, 73, 88-90, 104, 107, 126]. Regrettably, the computational complexity of an implementation is in the opposite order: KF is simplest, followed by EKF, followed by SPKF (theoretically the same order of complexity as EKF, but greater in complexity by a constant factor), followed by PF. This poses a tradeoff between accuracy and computational complexity that must be chosen to achieve the requirements of the application.

In addition to the technical considerations for choosing an estimator, there is an important legal consideration. There are a multitude of patents granted for methods of SOC estimation. At this point, it may be impossible to implement an SOC estimator without infringing on existing intellectual property. So, in addition to designing a robust and accurate technical solution, a favorable economic solution must be found by negotiating royalty rights.

4.2 Making adaptive-filter estimators reliable under different operating conditions

While I prefer adaptive-filter-based SOC estimators for the reasons articulated above, they will not always give satisfactory estimates until the algorithm designer takes some additional steps beyond implementing the basic algorithms themselves. For example, the designer must specify process-noise and sensor-noise covariance matrices, $\boldsymbol{\Sigma}_{\tilde{w}}$ and $\boldsymbol{\Sigma}_{\tilde{v}}$. If all of the assumptions made when deriving the adaptive-filter algorithms are met exactly, then $\boldsymbol{\Sigma}_{\tilde{w}}$ describes the uncertainty of unmeasured noise that affects the model state and $\boldsymbol{\Sigma}_{\tilde{v}}$

describes the uncertainty of the additive random noise in the voltage measurement. However, the derivation assumptions are never met exactly in practice, so $\boldsymbol{\Sigma}_{\tilde{w}}$ ultimately has the effect of describing in a summary way the state-equation inaccuracies, additional uncertainty in the filter because process noise and state uncertainty are not Gaussian, as well as the process noise itself; $\boldsymbol{\Sigma}_{\tilde{v}}$ ultimately has the effect of describing in a summary way the measurement-equation inaccuracies, additional uncertainty because the state uncertainty and measurement noise are not Gaussian, as well as the measurement noise itself. Consequently, it is essentially impossible to pre-compute $\boldsymbol{\Sigma}_{\tilde{w}}$ and $\boldsymbol{\Sigma}_{\tilde{v}}$ using an analytic procedure; instead, their values are usually hand-tuned by trial-and-error over many different operating scenarios to give satisfactory estimates with reliable error bounds. This is perhaps the most time-consuming and difficult part of implementing an adaptive-filter-based SOC estimator. However, a number of researchers have reported success with filters that adapt $\boldsymbol{\Sigma}_{\tilde{w}}$ and $\boldsymbol{\Sigma}_{\tilde{v}}$ along with the model state estimate: results using an adaptive extended Kalman filter (AEKF) are reported in [14, 47-48, 117-120]; results using an adaptive unscented Kalman filter (AUKF) are reported in [105].

A second challenge with xKF estimators is that the internal state-covariance matrices must remain symmetric and positive definite at all times. Theoretically, the algorithm guarantees this result; however, round-off numeric errors sometimes cause these matrices to lose symmetry and/or positive-definiteness. This can be corrected using a method from [138]. Suppose that $\boldsymbol{\Sigma}$ is the matrix under consideration. We then compute the singular-value decomposition $\boldsymbol{\Sigma}=\boldsymbol{USV}^{\mathrm{T}}$. Using the decomposition terms, we define $\boldsymbol{H}=\boldsymbol{VSV}^{\mathrm{T}}$ and finally replace $\boldsymbol{\Sigma}$ with $(\boldsymbol{\Sigma}+\boldsymbol{\Sigma}^{\mathrm{T}}+\boldsymbol{H}+\boldsymbol{H}^{\mathrm{T}})/4$. This procedure will guarantee that $\boldsymbol{\Sigma}$ is positive semi-definite (we would prefer positive definite, but this is still an improvement) and symmetric.

The xKF estimators also produce an internal covariance matrix of the expected voltage-prediction error. For the KF, $\boldsymbol{\Sigma}_{\tilde{y}}=\boldsymbol{C}_k\boldsymbol{\Sigma}_{\tilde{x},k}^{-}\boldsymbol{C}_k^{\mathrm{T}}+\boldsymbol{\Sigma}_{\tilde{v}}$; for EKF, $\boldsymbol{\Sigma}_{\tilde{y}}=\hat{\boldsymbol{C}}_k\boldsymbol{\Sigma}_{\tilde{x},k}^{-}\hat{\boldsymbol{C}}_k^{\mathrm{T}}+\boldsymbol{\Sigma}_{\tilde{v}}$; for SPKF, $\boldsymbol{\Sigma}_{\tilde{y},k}=\sum_{i=0}^{p}\alpha_i^{(\mathrm{c})}(\boldsymbol{\mathcal{Y}}_{k,i}-\hat{y}_k)(\boldsymbol{\mathcal{Y}}_{k,i}-\hat{y}_k)^{\mathrm{T}}$. In any of these cases, the covariance matrix may be used to check the quality of the estimate. Let $\sigma_{\tilde{y}}=\sqrt{\boldsymbol{\Sigma}_{\tilde{y}}}$ be the standard deviation of the expected voltage-prediction error. Then, observing $|y_k-\hat{y}_k|>3\sigma_{\tilde{y}}$ is expected to be an unlikely event, much less than 1% of the time. Observing $|y_k-\hat{y}_k|>6\sigma_{\tilde{y}}$ is an even more unlikely event, expected to occur by chance about one time in a million. Therefore, $\sigma_{\tilde{y}}$ can be used for two purposes: it can help detect voltage-sensor failures, and it can help detect when the state estimation-error covariance matrix $\boldsymbol{\Sigma}_{\tilde{x},k}^{+}$ has collapsed such that the state estimation-error covariance bounds are no longer descriptive of the true state uncertainty [98]. If the latter event is believed to have occurred, the state estimation-error covariance matrix can be artificially amplified by multiplying it by a positive scalar having value greater than 1. This will help the xKF to recover accurate confidence bounds.

Finally, the derivations of the xKF algorithms assume that sensors have no dc bias. This is not always true in practice. Sometimes, Hall-effect current sensors develop a hysteretic dc bias, for example, which can be slowly time varying and temperature-dependent and impossible to predict. If this is believed to be the case, additional states can be added to the cell model to describe the sensor biases, and these biases can be co-estimated along with the standard model states [87, 112-113]. This can greatly improve the SOC estimates.

4.3 What is the future?

By now, it should be evident that the field of SOC-estimation algorithms is very mature. Under controlled laboratory conditions, many of the methods are able to achieve estimation error lower than 1% routinely. In the field, a somewhat larger error is expected due to imperfect sensing systems and uncalibrated models, but even so, SOC estimates are generally quite good.

What remains to be done? It is difficult to predict the future with any accuracy, but I propose that there are three main areas that will produce fruitful research results in the coming years: new sensors, new materials, and new models.

4.3.1 New sensors

Traditional SOC-estimation methods rely on sensed voltage, current, and temperature. However, other measurable quantities have been shown to be correlated with cell SOC; for example, magnetism [139], strain [140–145], and ultrasound [146]. It is possible that these (or other) auxiliary measurements might be fused with standard measurements in an adaptive-filter-based SOC estimator to produce more reliable results.

4.3.2 New materials

Estimating SOC for cells having graphite anodes and cathodes comprising LMO, LCO, NMC, or NCA is relatively straightforward. Estimating SOC for LFP cells is more challenging because of the flatness of the OCV versus SOC relationship and because of hysteresis, but researchers have still reported good results, as mentioned earlier. However, future materials may pose additional challenges for SOC estimation. Cells having lithium-titanate-oxide (LTO) anodes coupled with LFP cathodes have extremely flat OCV versus SOC relationships (more so than graphite versus LFP), making it very difficult to estimate SOC well. And, there is an expectation that requirements of higher energy density will drive future cells to have silicon-based anodes.

Figure 13 shows measurements from a lab test performed on a cell having an NMC cathode and a silicon-based anode. This test discharged the cell from 100% SOC to 0% SOC at a C/30 rate. It then charged to 95%, discharged to 5%, and so forth, as shown in the left frame. The right frame shows voltage versus SOC for this test. Since the test was so slow, the cell was in a near-equilibrium state at every point in time. We see evidence of very strong hysteresis (path dependence in the resting voltage) for this test. For example, a resting cell voltage of 3.5 V might correspond to any SOC between about 5% and 45%.

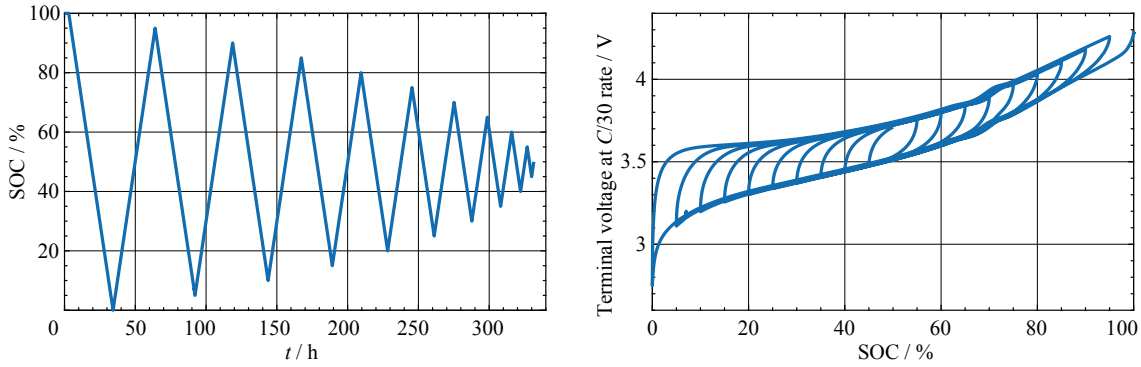

(a) SOC versus time for lab test (b) Evidence of hysteresis in silicon-anode cell

Figure 13 Evidence of hysteresis in a silicon-anode cell

In order to estimate SOC well for this type of cell, a very good model of hysteresis will be needed.

4.3.3 New models

As a final thought, we return to the fundamental question, "Why do we need an estimate of SOC?" We know that an estimate of SOC is an input to compute SOE, to some SOH methods, to balancing algorithms, and to SOP/SOF computations. Existing methods for existing cells compute SOC estimates that are sufficiently accurate for most SOE, SOH, and balancing procedures. But, there may be opportunities when considering future computations of power limits.

Power limits are presently computed to give authorization to the load or charger circuit for certain levels of power for a short predefined future time horizon such that cell terminal voltage will not exceed some predefined v_{max} or be lower than some predefined v_{min}. The objective of this exercise is to avoid causing damage to the cell by subjecting it to extreme voltages.

However, the terminal voltage of the cell is not actually a good indicator of the incremental aging that might occur over the specified future time horizon. Instead, the internal electrochemical state of the cell is a direct indicator of the conditions that cause premature aging and safety concerns. Equivalent-circuit models are not able to compute these internal electrochemical states; however, physics-based models can predict their values. State estimators using reduced-order physics-based lithium-ion cell models (e.g., [70]) can provide values for the internal electrochemical states that could be used by future power-limits estimators to compute physics-based power limits. In some cases it has been shown that PBM-based BMS can safely authorize 22 % more power than would be authorized by ECM-based BMS, provide more than 212 % more available energy, and that PBM-based BMS can extend battery-pack life by more than 40 % using intelligent state estimation and active balancing [147-148]. The use of physics-based models in BMS is still at a very early technology readiness level, but these results indicate that there is significant incentive to invest resources into research to determine whether they live up to their promise.

5 Summary

This paper has presented a sampling of the literature related to SOC estimation for lithium-ion batteries. One significant feature of this article has been showing that SOC is a physical quantity and so while engineering-SOC definitions may be very relevant to a particular application, it is a better practice to estimate the fundamental physical quantity first, and then to compute other quantities from that. The article then presented a taxonomy of the most common SOC-estimation methods reported in the literature and gave high-level descriptions regarding how each method works. This was followed by a section showing the need to estimate individual SOCs for every cell in a series-connected battery pack, and some efficient methods to do so. The discussion section presented some approaches to overcome challenges in implementing the SOC estimators, and some perspectives in the future. Overall, the field of algorithms for SOC-estimation is very mature, but there remain some avenues for future research that promise important benefits for some applications.

References / 参考文献

[1] Dhameja S. Electric Vehicle Battery Systems [M]. Newnes Press (an imprint of Butterworth-Heinemann), 2002, 47.

[2] Rodrigues S, Munichandraiah N, Shukla A. A review of state-of-charge indication of batteries by means of a.c. impedance measurements [J]. ***J Power Sources***, 2000, **87**(1-2): 12-20.

[3] Piller S, Perrin M, Jossen A. Methods for state-of-charge determination and their applications [J]. ***J Power Sources***, 2001, 96(1): 113-120.

[4] Pop V, Bergveld H J, Notten P, et al . State-of-the-art of battery state-of-charge determination [J]. ***Measurement Science and Technology***, 2005, **16**(12): R93-R110.

[5] CHANG Wen-Yeau. The state of charge estimating methods for battery: A review [J]. ***ISRN Appl Math***, 2013, 2013.

[6] LU Languang, HAN Xuebing, LI Jianqiu, et al. A review on the key issues for lithium-ion battery management in electric vehicles [J]. ***J Power Sources***, 2013, **226**: 272-288.

[7] XIONG Rui, CAO Jiayi, YU Quanqing, et al. Critical review on the battery state of charge estimation methods for electric vehicles

[J]. ***IEEE Access***, 2017, **6**: 1832-1843.

[8] Hannan M A, Lipu M H, Hussain A, et al. A review of lithium-ion battery state of charge estimation and management system in electric vehicle applications: Challenges and recommendations [J]. ***Renewable and Sustainable Energy Reviews***, 2017, **78**: 834-854.

[9] Vetter J, Novak P, Wagner M, et al. Ageing mechanisms in lithium-ion batteries [J]. ***J Power Sources***, 2005, 147: 269-281.

[10] Barré A, Deguilhem B, Grolleau S, et al. A review on lithium-ion battery ageing mechanisms and estimations for automotive applications [J]. ***J Power Sources***, 2013, **241**: 680-689.

[11] USABC. Glossary of battery and battery testing terminology for the USABC battery test procedures appendix F [C]// Electric Vehicle Battery Test Procedures Manual. USABC, 2009: 1-10.

[12] Truchot C, Dubarry M, Liaw B Y. State-of-charge estimation and uncertainty for lithium-ion battery strings [J]. ***Appl Energ***, 2014, **119**: 218-227.

[13] Chiasson J, Vairamohan B. Estimating the state of charge of a battery [C]// *Proc 2003 American Control Conference*. Denver cololorado, 2003, 4: 2863-2868.

[14] HE Hongwen, XIONG Rui, GUO Hongqiang. Online estimation of model parameters and state-of-charge of LiFePO4 batteries in electric vehicles [J]. ***Appl Energ***, 2012, **89**(1): 413-420.

[15] HE Hongwen, ZHANG Xiaowei, XIONG Rui, et al. Online model-based estimation of state-of-charge and open-circuit voltage of lithium-ion batteries in electric vehicles [J]. ***Energy***, 2012, **39**(1): 310-318.

[16] ZHENG Yuejiu, OUYANG Minggao, LU Languang, et al. Cell state-of-charge inconsistency estimation for $LiFePO_4$ battery pack in hybrid electric vehicles using mean-difference model [J]. ***Appl Energ***, 2013, **111**: 571-580.

[17] XING Yinjiao, HE Wei, Michael P, et al. State of charge estimation of lithium-ion batteries using the open-circuit voltage at various ambient temperatures [J]. ***Appl Energ***, 2014, **113**: 106-115.

[18] Dreyer W, Jamnik J, Guhlke C, et al. The thermodynamic origin of hysteresis in insertion batteries [J]. ***Nature materials***, 2010, **9**(5): 448-453.

[19] Sasaki T, Ukyo Y, Novák P. Memory effect in a lithium-ion battery [J]. ***Nature materials***, 2013, **12**(6): 569-575.

[20] Plett G L. Advances in EKF SOC estimation for LiPB HEV battery packs [C]// *Proc 20th Int'l Battery, Hybrid and Fuel Cell Electric Vehi Symp Exhib (EVS20).* Long Beach, CA, 2003.

[21] Plett G L. Extended Kalman filtering for battery management systems of LiPB-based HEV battery packs: Part 2. Modeling and identification [J]. ***J Power Sources***, 2004, **134**(2): 262-276.

[22] Roscher M A, Sauer D U. Dynamic electric behavior and open-circuit-voltage modeling of LiFePO4-based lithium ion secondary batteries [J]. ***J Power Sources***, 2011, **196**(1): 331-336.

[23] Schwunk S, Armbruster N, Straub S, et al. Particle filter for state of charge and state of health estimation for lithium–iron phosphate batteries [J]. ***J Power Sources***, 2013, **239**: 705-710.

[24] DONG Guangzhong, WEI Jingwen, ZHANG Chenbin, et al. Online state of charge estimation and open circuit voltage hysteresis modeling of $LiFePO_4$ battery using invariant imbedding method [J]. ***Appl Energ***, 2016, **162**: 163-171.

[25] NG Kong Soon, Moo Chin-Sien, Chen Yi-Ping, et al. Enhanced coulomb counting method for estimating state-of-charge and state-of-health of lithium-ion batteries [J]. ***Appl Energ***, 2009, **86**(9): 1506-1511.

[26] HU Xiaosong, LI Shengbo, PENG Huei, et al. Robustness analysis of state-of-charge estimation methods for two types of Li-ion batteries [J]. ***J Power Sources***, 2012, **217**: 209-219.

[27] Plett G L. Recursive approximate weighted total least squares estimation of battery cell total capacity [J]. ***J Power Sources***, 2011, **196**(4): 2319-2331.

[28] Kim Taesic, WANG Yebin, Zafer S, et al. A Rayleigh quotient-based recursive total-least-squares online maximum capacity estimation for lithium-ion batteries [J]. ***IEEE Trans Energy Conv***, 2015, **30**(3): 842-851.

[29] Dowgiallo Jr E J. Method for determining battery state of charge by measuring ac electrical phase angle change [P]. US Patent 3984762, 1976.

[30] Zaugg E. Process and apparatus for determining the state of charge of a battery [P]. US Patent 4433295, 1984,

[31] Westerhoff U, Kroker T, Kurbach K, et al. Electrochemical impedance spectroscopy based estimation of the state of charge of lithium-ion batteries [J]. ***J Energy Storage***, 2016, **8**: 244-256.

[32] Takano K, Nozaki K, Saito Y, et al. Simulation study of electrical dynamic characteristics of lithium-ion battery [J]. ***J Power Sources***, 2000, **90**(2): 214-23.

[33] Barsoukov E, Kim J, Yoon C, et al. Universal battery parameterization to yield a non-linear equivalent circuit valid for battery simulation at arbitrary load [J]. ***J Power Sources***, 1999, **83**(1-2): 61-70.

[34] Salkind A, Fennie C, Singh P, et al. Determination of state-of-charge and state-of-health of batteries by fuzzy logic methodology [J]. ***J Power Sources***, 1999, **80**(112): 293-300.

[35] Singh P C. Fennie J, Reisner D, et al. Fuzzy logic-enhanced electrochemical impedance spectroscopy (fleeis) to determine battery state of charge [C]// *Proc 15th Annual Battery Conf Appl Advances*. Long Beach, CA, USA, 2000: 199-204.

[36] XU Jun, MI Chunting Chris, CAO Binggang, DENG Junjun, CHEN Zheng, LI Siqi. The state of charge estimation of lithium-ion batteries based on a proportional-integral observer [J]. ***IEEE Trans Vehi Tech***, 2013, **63**(4): 1614-1621.

[37] Fleischer C, Wag W, Heyn H M, et al. On-line adaptive battery impedance parameter and state estimation considering physical principles in reduced order equivalent circuit battery models: Part 1. requirements, critical review of methods and modeling [J]. ***J Power Sources***, 2014, **260**: 276-291.

[38] Plett G L. Battery Management Systems, Volume I: Battery Modeling [M]. Boston: Artech House, 2015: 29-64.

[39] Plett G L, ECE5710: Modeling, simulation, and identification of battery dynamics [R/OL], University of Colorado Colorado Springs, [2019-08-22], http://mocha-java.uccs.edu/ECE5710/.

[40] Hansen T, Wang C J. Support vector based battery state of charge estimator [J]. ***J Power Sources***, 2005, **141**(2): 351-358.

[41] Antón J Á, Nieto P G, de Cos Juez F, et al. Battery state-of-charge estimator using the SVM technique [J]. ***Appl Math Mode***, 2013, **37**(9): 6244-6253.

[42] HU J N, HU J J, LIN H B, et al. State-of-charge estimation for battery management system using optimized support vector

machine for regression [J]. ***J Power Sources***, 2014, **269**: 682-693.

[43] HE Wei, Nicholas W, CHEN Chaochao, et al. State of charge estimation for Li-ion batteries using neural network modeling and unscented Kalman filter-based error cancellation [J]. ***Int'l J Electr Power Energ Syst***, 2014, **62**: 783-791.

[44] DANG Xuanju, YAN Li, XU Kai, et al. Open-circuit voltage-based state of charge estimation of lithium-ion battery using dual neural network fusion battery model [J]. ***Electrochimica Acta***, 2016, **188**: 356-366.

[45] Chemali E, Kollmeyer P J, Preindl M, et al. State-of-charge estimation of Li-ion batteries using deep neural networks: A machine learning approach [J]. ***J Power Sources***, 2018, **400**: 242-255.

[46] Plett G L. Kalman-filter SOC estimation for LiPB HEV cells [C]// *Proc 19th Int'l Battery, Hybrid Fuel Cell Electric Vehicle Symp Exhib (EVS19).* Busan, Korea, 2002, 527-538.

[47] Charkhgard M, Farrokhi M. State-of-charge estimation for lithium-ion batteries using neural networks and EKF [J]. ***IEEE Trans Ind Elect***, 2010, **57**(12): 4178-4187.

[48] SUN Fengchun, XIONG Rui, HE Hongwen. A systematic state-of-charge estimation framework for multi-cell battery pack in electric vehicles using bias correction technique [J]. ***Appl Energ***, 2016, **162**: 1399-1409.

[49] Schuster S F, Brand M J, Campestrini C, et al. Correlation between capacity and impedance of lithium-ion cells during calendar and cycle life [J]. ***J Power Sources***, 2016, **305**: 191-199.

[50] HU Xiaosong, LI Shengbo, PENG Huei. A comparative study of equivalent circuit models for Li-ion batteries [J]. ***J Power Sources***, 2012, **198**: 359-367.

[51] Rodriguez A, Plett G L. Controls-oriented models of lithium-ion cells having blend electrodes. part 2: Physics-based reduced-order models [J]. ***J Energy Storage***, 2017, **11**: 219-236.

[52] WANG Baojin, LI Shengbo Eben, PENG Huei, et al. Fractional-order modeling and parameter identification for lithium-ion batteries [J]. ***J Power Sources***, 2015, **293**: 151-161.

[53] Doyle M, Fuller T F, Newman J. Modeling of galvanostatic charge and discharge of the lithium/polymer/insertion cell [J]. ***J Electrochemical Society***, 1993, **140**(6): 1526-1533.

[54] Santhanagopalan S, White R E. Online estimation of the state of charge of a lithium ion cell [J]. ***J Power Sources***, 2006, **161**(2): 1346-1355.

[55] Moura S J, Krstić M, Chaturvedi N A. Adaptive PDE observer for battery SOC/SOH estimation [C]// *Proc 2012 ASME Dynamic Systems and Control Conf.* Fort Lauderdale, 2012: 101-110.

[56] Moura S J, Chaturvedi N A, Krstić M. PDE estimation techniques for advanced battery management systems—Part I: SOC estimation [C]// *Proc 2012 American Control Conf.* Montreal, Canada, 2012: 559-565.

[57] Moura S J, Chaturvedi N A, Krstić M. Adaptive partial differential equation observer for battery state-of-charge/state-of-health estimation via an electrochemical model [J]. ***J Dyna Syst, Meas Contr***, 2014, **136**(1): 011015.

[58] Moura S J. Estimation and control of battery electrochemistry models: A tutorial [C]// *Proc 54th IEEE Conference on Decision and Control,* Osaka, Japan, 2015: 3906-3912.

[59] Bartlett A, Marcicki J, Onori S, et al. Model-based state of charge estimation and observability analysis of a composite electrode lithium-ion battery [C]// *Proc 52nd IEEE Conference on Decision and Control.* Florence, Italy, 2013: 7791-7796.

[60] Tanim T R, Rahn C D, Wang C Y. State of charge estimation of a lithium ion cell based on a temperature dependent and electrolyte enhanced single particle model [J]. ***Energy***, 2015, **80**: 731-739.

[61] Bartlett A, Marcicki J, Onori S, et al. Electrochemical model-based state of charge and capacity estimation for a composite electrode lithium-ion battery [J]. ***IEEE Trans Contr Syst Tech***, 2015, **24**(2): 384-399.

[62] Di Domenico D, Fiengo G, Stefanopoulou A. Lithium-ion battery state of charge estimation with a Kalman filter based on a electrochemical model [C]// *Proc 2008 IEEE Int'l Conf Control Applications.* San Antonio, TX. 2008: 702-707.

[63] Smith K A, Rahn C D, Wang C Y. Model-based electrochemical estimation of lithium-ion batteries [C]// *Proc 2008 IEEE Int'l Conf Control Applications.* San Antonio, TX, 2008: 714-719.

[64] Smith K A, Rahn C D, Wang C Y. Model-based electrochemical estimation and constraint management for pulse operation of lithium ion batteries [J]. ***IEEE Trans Contr Syst Tech***, 2009, **18**(3): 654-663.

[65] Santhanagopalan S, White R E. State of charge estimation using an unscented filter for high power lithium ion cells [J]. ***Int'l J Energ Res***, 2010, **34**(2): 152-163.

[66] Di Domenico D, Stefanopoulou A, Fiengo G. Lithium-ion battery state of charge and critical surface charge estimation using an electrochemical model-based extended Kalman filter [J]. ***J Dyna Syst, Meas, Contr***, 2010, **132**(6): 061302.

[67] Suthar B, Ramadesigan V, Northrop P W, et al. Optimal control and state estimation of lithium-ion batteries using reformulated models [C]// *Proc 2013 American Contr Conf.* Washington, DC. 2013: 5350-5355.

[68] HAN Xuebing, OUYANG Minggao, LU Languang, et al. Simplification of physics-based electrochemical model for lithium ion battery on electric vehicle. part ii: Pseudo-two-dimensional model simplification and state of charge estimation [J]. ***J Power Sources***, 2015, **278**: 814-825.

[69] Bizeray A M, Zhao S, Duncan S R, et al. Lithium-ion battery thermal-electrochemical model-based state estimation using orthogonal collocation and a modified extended Kalman filter [J]. ***J Power Sources***, 2015, **296**: 400-412.

[70] Stetzel K D, Aldrich L L, Trimboli M S, et al. Electrochemical state and internal variables estimation using a reduced-order physics-based model of a lithium-ion cell and an extended Kalman filter [J]. ***J Power Sources***, 2015, **278**: 490-505.

[71] Sturm J, Ennifar H, Erhard S V, et al. State estimation of lithium-ion cells using a physicochemical model based extended Kalman filter [J]. ***Appl Energ***, 2018, **223**: 103-123.

[72] Roscher M A, Bohlen O S, Sauer D U. Reliable state estimation of multicell lithium-ion battery systems [J]. ***IEEE Trans Energ Conv***, 2011, **26**(3): 737-743.

[73] LI Jiahao, Klee B J, Clemens G, et al. A comparative study of state of charge estimation algorithms for $LiFePO_4$ batteries used in electric vehicles [J]. ***J Power Sources***, 2013, **230**: 244-250.

[74] WANG Baojin, LIU Zhiyuan, LI Shengbo Eben, et al. State-of-charge estimation for lithium-ion batteries based on a nonlinear

fractional model [J]. ***IEEE Trans Contr Syst Tech***, 2016, **25**(1): 3-11.

[75] Zou C, Hu X, Dey S, et al. Nonlinear fractional-order estimator with guaranteed robustness and stability for Lithium-Ion batteries [J]. ***IEEE Trans Indu Electr***, 2018, **65**(7): 5951-5961.

[76] Kim I S. The novel state of charge estimation method for lithium battery using sliding mode observer [J]. ***J Power Sources***, 2006, **163**(1): 584-590.

[77] ZHANG Fei, LIU Guangjun, FANG Lijin. A battery state of charge estimation method using sliding mode observer [C]// *Proc 7th World Congress on Intelligent Control and Automation*. Chang qing, China, 2008: 989-994.

[78] Belhani A, M' Sirdi N K, Naamane A. Adaptive sliding mode observer for estimation of state of charge [J]. ***Energy Procedia***, 2013 (42): 377-386.

[79] CHEN Xiaopeng, SHEN Weixiang, CAO Zhenwei, et al. A novel approach for state of charge estimation based on adaptive switching gain sliding mode observer in electric vehicles [J]. ***J Power Sources***, 2014, **246**: 667-678.

[80] NING Bo, XU Jun, CAO Binggang, et al. A sliding mode observer SOC estimation method based on parameter adaptive battery model [J]. ***Energy Procedia***, 2016, **88**: 619-626.

[81] ZHONG Qishui, ZHONG Fuli, CHENG Jun, et al. State of charge estimation of lithium-ion batteries using fractional order sliding mode observer [J]. ***ISA transactions***, 2017, **66**: 448-459.

[82] NING Bo, CAO Binggang, WANG Bin, et al. Adaptive sliding mode observers for lithium-ion battery state estimation based on parameters identified online [J]. ***Energy***, 2018, **153**: 732-742.

[83] Lürkens P, Steffens W. Ladezustandsschätzung von bleibatterien mit hilfe des kalman-filters (In German. English title: State of charge estimation of lead-acid batteries using a Kalman filtering technique) [J]. ***etzArchiv***, 1986, **8**(7): 231-236.

[84] Barbier C, Meyer H, Nogarede B, et al. A battery state of charge indicator for electric vehicle [C]. Institution of Mechanical Engineers Conference Publications. Medical Engineering Publications Ltd, 1994(5): 29-34.

[85] PANG Shuo, Jay F, DU Jie, et al. Battery state-of-charge estimation [C]// *Proc 2001 American Contr Conf.* Arlington, VA, 2001(2): 1644-1649.

[86] Plett G L, ECE5550: Applied Kalman filtering [R/OL]. University of Colorado Colorado Springs. [2019-08-22], http://mocha-java.uccs.edu/ECE5550/.

[87] LIU Xingtao, CHEN Zonghai, ZHANG Chenbin, et al. A novel temperature-compensated model for power Li-ion batteries with dual-particle-filter state of charge estimation [J]. ***Appl Energ***, 2014, **123**: 263-272.

[88] WANG Yujie, ZHANG Chenbin, CHEN Zonghai. A method for joint estimation of state-of-charge and available energy of $LiFePO_4$ batteries [J]. ***Appl Energ***, 2014, **135**: 81-87.

[89] WANG Yujie, ZHANG Chenbin, CHEN Zonghai. A method for state-of-charge estimation of $LiFePO_4$ batteries at dynamic currents and temperatures using particle filter [J]. ***J Power Sources***, 2015, **279**: 306-311.

[90] YANG Fangfang, XING Yinjiao, WANG Dong, et al. A comparative study of three model-based algorithms for estimating state-of-charge of lithium-ion batteries under a new combined dynamic loading profile [J]. ***Appl Energ***, 2016, **164**: 387-399.

[91] YE Min, GUO Hui, CAO Binggang. A model-based adaptive state of charge estimator for a lithium-ion battery using an improved adaptive particle filter [J]. ***Appl Energ***, 2017, **190**: 740-748.

[92] Kalman R. A new approach to linear filtering and prediction problems [J]. ***Trans ASME—J Basic Engineering***, 1960, 82, Series D: 35-45.

[93] The Seminal Kalman Filter Paper (1960) [R/OL], (download time? [2019-08-22], http://www.cs.unc.edu/welch/kalman/kalmanPaper.html.

[94] Haykin S. Kalman Filtering and Neural Networks [C] // Kalman Filters (Haykin S, editor). Wiley Inter-Science, New York, 2001: 1-22.

[95] Haykin S. Adaptive Filter Theory (3 edit) [M]. Prentice Hall, Upper Saddle River, NJ, 1996: 302-337.

[96] Burl J. Linear Optimal Control: H_2 and H_∞ Methods [M]. Addison Wessley, Menlo Park, CA, 1999: 231-279.

[97] XU Jun, Chris M C, CAO Binggang, et al. A new method to estimate the state of charge of lithium-ion batteries based on the battery impedance model [J]. ***J Power Sources***, 2013, **233**:277-284.

[98] Plett G L. Battery Management Systems, Volume II: Equivalent-Circuit Methods [M]. Artech House, US, 2015: 69-166.

[99] Plett G L, ECE5720: Battery management and control [R/OL], University of Colorado Colorado Springs, [2019-08-22], http://mocha-java.uccs.edu/ECE5720/.

[100] Plett G L. Extended Kalman filtering for battery management systems of LiPB-based HEV battery packs: Part 1. Background [J]. ***J Power Sources***, 2004, **134**(2): 252-261.

[101] Plett G L. Extended Kalman filtering for battery management systems of LiPB-based HEV battery packs: Part 2. State and parameter estimation [J]. ***J Power Sources***, 2004, **134**(2): 277-292.

[102] HU Chao, Byeng D Y, Jaesik C. A multiscale framework with extended Kalman filter for lithium-ion battery SOC and capacity estimation [J]. ***Appl Energ***, 2012, **92**: 694-704.

[103] HU Xiaosong, SUN Fengchun, ZOU Yuan. Comparison between two model-based algorithms for Li-ion battery SOC estimation in electric vehicles [J]. ***Simulation Modelling Practice and Theory***, 2013, **34**: 1-11.

[104] WANG Yujie, ZHANG Chenbin, CHEN Zonghai. A method for state-of-charge estimation of Li-ion batteries based on multi-model switching strategy [J]. ***Appl Energ***, 2015, **137**: 427-434.

[105] XIE Shanshan, XIONG Rui, ZHANG Yongzhi, et al. The estimation of state of charge for power battery packs used in hybrid electric vehicle [J]. ***Energy Procedia***, 2017, **105**: 2678-2683.

[106] ZOU Yuan, HU Xiaosong, MA Hongmin, et al. Combined state of charge and state of health estimation over lithium-ion battery cell cycle lifespan for electric vehicles [J]. ***J Power Sources***, 2015, **273**: 793-803.

[107] SHEN Yanqing. Adaptive extended Kalman filter based state of charge determination for lithium-ion batteries [J]. ***Electrochimica Acta***, 2018, **283**: 1432-1440.

[108] OUYANG Minggao, LIU Guangming, LU Languang, et al. Enhancing the estimation accuracy in low state-of-charge area:

A novel onboard battery model through surface state of charge determination [J]. ***J Power Sources***, 2014, **270**: 221-237.

[109] ZHENG Yuejiu, GAO Wenkai, OUYANG Minggao, et al. State-of-charge inconsistency estimation of lithium-ion battery pack using mean-difference model and extended Kalman filter [J]. ***J Power Sources***, 2018, **383**: 50-58.

[110] ZHANG Xu, WANG Yujie, YANG Duo, et al. An on-line estimation of battery pack parameters and state-of-charge using dual filters based on pack model [J]. ***Energy***, 2016, 115: 219-229.

[111] DAI Haifeng, WEI Xuezhe, SUN Zechang, et al. Online cell SOC estimation of Li-ion battery packs using a dual time-scale Kalman filtering for EV applications [J]. ***Appl Energ***, 2012, **95**: 227- 237.

[112] ZHAO Shi, Stephen D R, David H A. Observability analysis and state estimation of lithium-ion batteries in the presence of sensor biases [J]. ***IEEE Trans Contr Syst Tech***, 2016, **25**(1): 326-333.

[113] Plett G L. Efficient battery pack state estimation using bar-delta filtering [C]// *Proc 24th Int'l Battery, Hybrid and Fuel Cell Electric Vehicle Symp Exhib (EVS24).* Stavanger, Norway, 2009: 1-8.

[114] XIAO Renxin, SHEN Jiangwei, LI Xiaoyu, et al. Comparisons of modeling and state of charge estimation for lithium-ion battery based on fractional order and integral order methods [J]. ***Energies***, 2016, **9**(3): 184-199.

[115] FANG Huazhen, ZHAO Xin, WANG Yebin, et al. Improved adaptive state-of-charge estimation for batteries using a multi-model approach [J]. ***J Power Sources***, 2014, **254**: 258-267.

[116] HE Hongwen, XIONG Rui, FAN Jinxin. Evaluation of lithium-ion battery equivalent circuit models for state of charge estimation by an experimental approach [J]. ***Energies***, 2011, **4**(4): 582-598.

[117] XIONG Rui, HE Hongwen, SUN Fengchun, et al. Evaluation on state of charge estimation of batteries with adaptive extended Kalman filter by experiment approach [J]. ***IEEE Trans Vehi Tech***, 2012, **62**(1): 108-117.

[118] SUN Fengchun, XIONG Rui. A novel dual-scale cell state-of-charge estimation approach for series-connected battery pack used in electric vehicles [J]. ***J Power Sources***, 2015, **274**: 582-594.

[119] HE Hongwen, XIONG Rui, ZHANG Xiaowei, et al. State-of-charge estimation of the lithium-ion battery using an adaptive extended Kalman filter based on an improved Thevenin model [J]. ***IEEE Trans Vehi Tech***, 2011, **60**(4): 1461-1469.

[120] XIONG Rui, SUN Fengchun, GONG Xianzhi, et al. A data-driven based adaptive state of charge estimator of lithium-ion polymer battery used in electric vehicles [J]. ***Appl Eneryg***, 2014, **113**:1421-1433.

[121] Plett G L. Sigma-point Kalman filtering for battery management systems of LiPB-based HEV battery packs: Part 1: Introduction and state estimation [J]. ***J Power Sources***, 2006, **161**(2): 1356-1368.

[122] Plett G L. Sigma-point Kalman filtering for battery management systems of LiPB-based HEV battery packs: Part 2: Simultaneous state and parameter estimation [J]. ***J Power Sources***, 2006, **161**(2): 1369-1384.

[123] ZHENG Fangdan, XING Yinjiao, JIANG Jiuchun, et al. Influence of different open circuit voltage tests on state of charge online estimation for lithium-ion batteries [J]. ***Appl Energy***, 2016, **183**: 513-525.

[124] Andre D, Appel C, Soczka-Guth T, et al. Advanced mathematical methods of SOC and SOH estimation for lithium-ion batteries [J]. ***J Power Sources***, 2013, **224**: 20-27.

[125] SUN Fengchun, HU Xiaosong, ZOU Yuan, et al. Adaptive unscented Kalman filtering for state of charge estimation of a lithium-ion battery for electric vehicles [J]. ***Energy***, 2011, **36**(5): 3531-3540.

[126] HE Wei, Nicholas W, CHEN Chaochao, et al. State of charge estimation for electric vehicle batteries using unscented Kalman filtering [J]. ***Microelectronics Reliability***, 2013, **53**(6): 840-847.

[127] HE Zhigang, CHEN Dong, PAN Chaofeng, et al. State of charge estimation of power Li-ion batteries using a hybrid estimation algorithm based on UKF [J]. ***Electrochimica Acta***, 2016, **211**: 101-109.

[128] TIAN Yong, XIA Bizhong, SUN Wei, et al. A modified model based state of charge estimation of power lithium-ion batteries using unscented Kalman filter [J]. ***J Power Sources***, 2014, **270**: 619-626.

[129] ZHONG Liang, ZHANG Chenbin, HE Yao, et al. A method for the estimation of the battery pack state of charge based on in-pack cells uniformity analysis [J]. ***Appl Energy***, 2014, **113**: 558-564.

[130] LI Di, OUYANG Jian, LI Huiqi, et al. State of charge estimation for LiMn2O4 power battery based on strong tracking sigma point Kalman filter [J]. ***J Power Sources***, 2015, **279**: 439-449.

[131] MU Hao, XIONG Rui, ZHENG Hongfei, et al. A novel fractional order model based state-of-charge estimation method for lithium-ion battery [J]. ***Appl Energy***, 2017, **207**: 384-393.

[132] ZHANG Fei, LIU Guangjun, FANG Lijin, et al. Estimation of battery state of charge with H_∞ observer: Applied to a robot for inspecting power transmission lines [J]. ***IEEE Trans Indu Electronics***, 2011, **59**(2): 1086-1095.

[133] LIN Cheng, MU Hao, XIONG Rui, et al. A novel multi-model probability battery state of charge estimation approach for electric vehicles using H-infinity algorithm [J]. ***Appl Energy***, 2016, **166**: 76-83.

[134] CHEN Cheng, SUN Fengchun, XIONG Rui, et al A novel dual H infinity filters based battery parameter and state estimation approach for electric vehicles application [J]. ***Energy Procedia***, 2016, **103**: 375-380.

[135] HUA Yin, Cordoba-Arenas Andrea, Nicholas W, et al. A multi time-scale state-of-charge and state-of-health estimation framework using nonlinear predictive filter for lithium-ion battery pack with passive balance control [J]. ***J Power Sources***, 2015, **280**: 293-312.

[136] Plett G. High-performance battery-pack power estimation using a dynamic cell model [J]. ***IEEE Trans Vehi Tech***, 2004, **53**(5): 1586-1593.

[137] ZHANG Caiping, WANG Le Yi, LI Xue, et al. Robust and adaptive estimation of state of charge for lithium-ion batteries [J]. ***IEEE Tran Indu Electr***, 2015, **62**(8): 4948-4957.

[138] Higham N J. Computing a nearest symmetric positive semidefinite matrix [J]. ***Linear Algebra and Its Applications***,

1988, **103**: 103-118.

[139] Gallien T, Krenn H, Fischer R, Lauterbach S, Schweighofer B, Wegleiter H. Magnetism versus LiFeP04 battery's state of charge: A feasibility study for magnetic-based charge monitoring [J]. ***IEEE Transactions on Instrumentation and Measurement***, 2015, **64**(11): 2959-2964.

[140] ZHU Yujie, WANG Chunsheng. Strain accommodation and potential hysteresis of lifepo4 cathodes during lithium ion insertion/extraction [J]. ***J Power Sources***, 2011, **196**(3): 1442-1448.

[141] Mohan S, Kim Y, Siegel J B, et al. A phenomenological model of bulk force in a li-ion battery pack and its application to state of charge estimation [J]. ***J Electrochemical Society***, 2014, **161**(14): A2222-A2231.

[142] Cannarella J, Arnold C B. State of health and charge measurements in lithium-ion batteries using mechanical stress [J]. ***J Power Sources***, 2014, **269**: 7-14.

[143] Ganguli A, Saha B, Raghavan A, et al. Embedded fiber-optic sensing for accurate internal monitoring of cell state in advanced battery management systems part 2: Internal cell signals and utility for state estimation [J]. ***J Power Sources***, 2017, **341**: 474-482.

[144] Raghavan A, Kiesel P, Sommer L W, et al. Embedded fiber-optic sensing for accurate internal monitoring of cell state in advanced battery management systems part 1: Cell embedding method and performance [J]. ***J Power Sources***, 2017, **341**: 466-473.

[145] Ladpli P, Kopsaftopoulos F, Chang F K. Estimating state of charge and health of lithium-ion batteries with guided waves using built-in piezoelectric sensors/actuators [J]. ***J Power Sources***, 2018, **384**: 342-354.

[146] Gold L, Bach T, Virsik W, et al. Probing lithium-ion batteries' state-of-charge using ultrasonic transmission–Concept and laboratory testing [J]. ***J Power Sources***, 2017, **343**: 536-544.

[147] Smith K A, Wang C Y. Power and thermal characterization of a lithium-ion battery pack for hybrid-electric vehicles [J]. ***J Power Sources***, 2006, **160**: 662-673.

[148] Anderson R, Zane R, Plett G, et al. Life balancing—a better way to balance large batteries [R]. **SAE Tech Paper**. 2017-01-1210, 2017.

[149] Wan E, Nelson A. Kalman Filtering and Neural Networks [C]// Dual extended Kalman filter methods (Haykin S, editor). Wiley Inter-Science, New York, 2001: 123-174.

Prof. Dr. Gregory L. PLETT

Prof. Dr. Gregory PLETT received his Ph.D. in Electrical Engineering from Stanford University in 1998. Since that time, he has been a faculty member in the *Department of Electrical and Computer Engineering at the University of Colorado Colorado Springs*, where he is now Professor. He has been an active researcher in the field of algorithms for battery management systems since 2001. He was an early pioneer of using Kalman-filter methods for SOC estimation. He and his students are now focusing their research on reduced-order physics-based models of lithium-ion cells, including parameter identification, degradation modeling, and optimized power and energy estimation to enhance safety and extend life.

Gregory L. PLETT 教授

1998 年在斯坦福大学电子工程系获得博士学位。之后他获得科罗拉多大学（科罗拉多斯普林斯）电气及计算机工程系的教职，现在任教授。从 2001 年起他就活跃在电池管理系统算法的研究领域，他是将 Kalman 滤波算法用于电荷状态（SOC）估算的开创者。他的团队目前的研究集中在基于降阶的、基于物理的锂离子电池模型上，具体包括参数识别、退化建模以及功率和能量优化估算，以达到提高电池安全并延长寿命的目的。